ABSTRACT

IN-VITRO CHARACTERIZATION OF BORONIZED TITANIUM ALLOY BY MEANS OF CORROSION AND ELECTROCHEMICAL IMPEDANCE SPECTROSCOPY METHODS IN SIMULATED BODY FLUIDS

by

David Anthony Panus

Titanium and titanium alloys are becoming the backbone of medical implants and prosthetics. Titanium alloys are used because of its high biocompatibility and similarity to bone. However, titanium and titanium alloys have a low wear resistance. Titanium and titanium alloys are susceptible to particle erosion, which can cause inflammation, infection, and even implant rejection. Boronizing titanium alloy improves titanium's wear resistance and also improves corrosion resistance.

The target of this research was to characterize the corrosion characteristics of both unboronized and boronized titanium using both electrochemical corrosion methods and Electrochemical Impedance Spectroscopy (EIS) in simulated body fluid. Using electrochemical methods the corrosion rate of boronized titanium decreased from 1.5 x 10^{-4} MPY to 8.67 x 10^{-5} MPY, while the corrosion rate of unboronized titanium decreased from 1.62 x 10^{-4} MPY to 3.42 x 10^{-6} MPY. Unboronized titanium alloy exhibited pitting corrosion while boronized titanium remained unchanged. EIS testing for boronized titanium alloy proved the existence of a protective layer, while the unboronized titanium alloy exhibited the formation of a passive layer over the course of testing. Moreover, boronized titanium alloy has shown an ability to withstand corrosive environments and pitting corrosion, which was not seen in unboronized titanium alloy.

IN-VITRO CHARACTERIZATION OF BORONIZED TITANIUM ALLOY BY MEANS OF CORROSION AND ELECTROCHEMICAL IMPEDANCE SPECTROSCOPY METHODS IN SIMULATED BODY FLUIDS

by
David Anthony Panus

A Thesis
Submitted to the Faculty of
New Jersey Institute of Technology
In Partial Fulfillment of the Requirements for the Degree of
Master of Science in Biomedical Engineering

Department of Biomedical Engineering

August 2006

APPROVAL PAGE

IN-VITRO CHARACTERIZATION OF BORONIZED TITANIUM ALLOY BY MEANS OF CORROSION AND ELECTROCHEMICAL IMPEDANCE SPECTROSCOPY METHODS IN SIMULATED BODY FLUIDS

David Anthony Panus

Dr. Reginald Tomkins, Thesis Committee Chair — Date
Professor of Chemical Engineering, NJIT

Dr. Roumiana S. Petrova, Thesis Advisor — Date
Special Lecturer of Chemistry, NJIT

Dr. Bryan Pfister, Committee Member — Date
Assistant Professor of Biomedical Engineering, NJIT

BIOGRAPHICAL SKETCH

Author: David Anthony Panus

Degree: Master of Science

Date: August 2006

Undergraduate and Graduate Education:

- Master of Science in Biomedical Engineering,
  New Jersey Institute of Technology, Newark, NJ, 2006

- Bachelor of Science in Biomedical Engineering,
  New Jersey Institute of Technology, Newark, NJ, 2005

Major: Biomedical Engineering

To my beloved family and friends, I never would have been able to do this without your love and support; you make me who I am.

ACKNOWLEDGEMENT

I would first like to thank Dr. Roumiana S. Petrova, for all of her attention, support, and understanding, and giving me this opportunity to work with her. I would also like to give special thanks to Dr. Reginald Tomkins and Dr. Bryan Pfister for their guidance, and participations on my thesis committee.

A very special thanks to Naruemon Suwattananont for all of her time and patience during those long hours training me on laboratory procedures. I would also like to thank Joel Payne, and Steve Zlatev for all of their time and effort in assisting my research, and Liz Vailhe for putting my school work before everything else.

I would like to thank my parents, and brothers Ed, and Mike, for never giving up on me and putting up with me when times were rough. Thanks to Jon and Nichole for listening to my scientific explanations on how the world works.

Finally I would like to thank my fiancée, Sarah. You are my everything and with you I can achieve anything because with you failure does not exist. To each and everyone -- I thank you.

TABLE OF CONTENTS

TABLE OF CONTENTS
(Continued)

Chapter **Page**

TABLE OF CONTENTS
(Continued)

Chapter **Page**

TABLE OF CONTENTS
(Continued)

TABLE OF CONTENTS
(Continued)

LIST OF TABLES

LIST OF TABLES
(Continued)

LIST OF FIGURES

LIST OF FIGURES
(Continued)

LIST OF FIGURES
(Continued)

CHAPTER 1

INTRODUCTION

1.1 Objective

The purpose of this research study is to understand the biocompatibility of boronized titanium in biomedical applications. Current biomedical applications use titanium and titanium alloys such as Ti-6Al-4V because of their high affinity for biocompatibility. However, titanium and titanium alloys have a low wear resistance making them susceptible to malfunction. Ti-6Al-4V was used in this study because of its current widespread use in biomedical applications, such as hip and knee replacements and in many dental applications. Ti-6Al-4V is also widely available and is relatively low cost.

1.2 Background Information

Boronization is a thermo-chemical process known to increase the hardness and wear resistance of many metals. Boronization occurs when boron atoms diffuse into the surface of a metal and form a boride layer; titanium alloys form titanium boride (TiB) and titanium diboride (TiB_2) layers. There are a number of boronization techniques currently used including: pack boriding, solid phase boriding, paste boriding, liquid phase boriding, gaseous phase boriding, plasma phase boriding, fluidized bed boriding, and multicomponent boriding [9]. Each has benefits and limitations. Paste and packing methods of boronization are the most easily used because they can be applied to many applications, but they can also be time consuming. Other techniques like liquid phase and gaseous phase boriding can produce hazardous by-products in the form of lethal

gases, such as HCl and HF fumes [9]. Pack boronization was used because of the simplicity, low cost, and the ability to control the thickness of the boride layer.

Boriding's attractive properties include a high melting point, high hardness, good wear and corrosion resistance, and excellent electrical conductivity [9]. These properties make the application to the surface of titanium ideal for use in biomedical applications.

1.3 Applications for Boronization

Borided materials have many useful applications other than biomedical implants. For example, most manufacturing processes require the use of stamps and cutting dies. Repetitive stamping can cause metal fatigue and dull die blade edges. Boriding the cutting stamps and dies increases the blade life. Boriding is also being used in nuclear applications such as lining of nuclear reactors, and can be applied to increase electrical conductor's temperature threshold at which the wiring can be used. Conventional thermistors only operate at 300°C; boriding the metal wiring could increase the operation temperature to approximately 800°C.

CHAPTER 2

TITANIUM

2.1 Metallurgy of Titanium

The properties of titanium and titanium alloys are dependent on their basic structure, and the mechanical and thermal treatments used during manufacturing [3]. Titanium is an allotropic element, which means titanium exists in more than one crystallographic form. At lower temperatures (22-882°C) titanium exists as a hexagonal close-packed (hcp) crystal structure, which is also referred to as the "alpha" (α) phase. At higher temperatures (883°C and above), the structure of titanium transitions from the hexagonal close-packed crystal structure to a body-centered cubic (bcc) crystal structure, which is also referred to as the "beta" (β) phase [2].

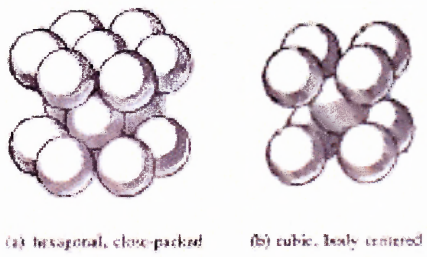

Figure 2.1 Crystal structure of titanium in alpha and beta phases [2].

2.2 Metallurgy of Titanium Alloys

The transformation of titanium from the alpha phase to the beta phase can be modified through the addition of alloying elements (aluminum, tin, vanadium, molybdenum, chromium, copper, zirconium, and silicon) which will produce alloys that have all α, β, or α+β structures at room temperature [3]. An alpha alloy does not form a beta phase, and vice versa because alpha alloys are unstable at higher temperature, and beta alloys do not form an alpha phase again because beta alloys are not stable at low temperatures . An alpha-beta alloy, as in the case of titanium, consists of alpha and retained or transformed beta because aluminum is an alpha stabilizer and vanadium is a beta stabilizer. Alloy element identification as alpha and beta stabilizers is shown in Table 2.1

Table 2.1 Ranges and Effects of Alloying Elements Used in Titanium [2]

Alloying Element	Range (approx.) wt%	Effect on Structure
Aluminum	2 to 7	Alpha Stabilizer
Tin	2 to 6	Alpha Stabilizer
Vanadium	2 to 20	Beta Stabilizer
Molybdenum	2 to 20	Beta Stabilizer
Chromium	2 to 12	Beta Stabilizer
Copper	2 to 6	Beta Stabilizer
Zirconium	2 to 8	Alpha and Beta Strengthener
Silicon	0.2 to 1	Improve creep resistance

Alpha stabilizers, such as aluminum and tin, increase the temperature at which the α phase is stable. Beta stabilizers, like vanadium and chromium, add stability to the β phase at lower temperatures. An alloy containing both alpha and beta stabilizers (α+β alloy) is more desirable than just an alpha (α) or beta (β) alloy, this is because an α+β alloy is stable over a wider range of temperatures. An alpha alloy is only stable at lower

temperatures while beta alloys are only stable in higher temperatures. Since Ti-6Al-4V contains of aluminum an alpha stabilizer and vanadium which is a beta stabilizer, Ti-6Al-4V is an $\alpha+\beta$ alloy.

Table 2.2 Properties of Ti-6Al-4V [8]

Ti-6Al-4V Properties	
Property	**Value**
Specific Gravity	4.4
Tensile Strength	130,000 lb/in^2
Strength to Weight Ratio	29,000
Yield Strength	130 ksi
Elongation	17%
Elastic Modulus	110 GPa
Smooth Fatigue Limit	500 MPa

2.3 Advantages and Limitations of Ti-6Al-4V

Advantages:

- Presence of β phase improves formability, forgeability, and strength at low total alloy contents. Added vanadium strengthens β phase.
- Added aluminum increases strength and creep resistance of α phase.
- By heating an alloy to a specific temperature either the α or β portion of the alloy can dominate. At low temperatures the α portion of the alloy dominates, at higher temperatures the β portion dominates.
- $\alpha + \beta$ alloys with fine structure are superplastic, enabling complex shapes to be formed.
- Reduction in β phase content increases creep resistance by reducing β stabilizers.

Limitations:

- Higher alloy contents reduce formability but better hardenability.
- Increase in alloying metals decreases ductility, and forgeability.
- Need to forge alloy or process in $\alpha+\beta$ range to ensure both α and β portions are processed.
- Strain rates for superplastic forming very low; argon atmosphere (or vacuum) needed to avoid surface contamination or alternation.
- Lower strength at ambient temperature. Lower depth of hardening with fewer β stabilizers.

CHAPTER 3

BORONIZING

3.1 Boronizing

Boronizing can be applied to many metals and metal alloys. During boronization, boron atoms diffuse into the metal substrate and combine with the atoms of the metal substrate [9]. The combined metal and boron atoms in the substrate form single-phase boride or multiphase boride layers. In the case of titanium, both titanium boride (TiB) and titanium diboride (TiB_2) are formed. All boronizing techniques are carried out at temperatures of 700-1000°C. The treatment lasts for several hours depending on the desired thickness of the boride layer. Boronizing can produce a hard layer 50-150μm thick. Not all metals can be boronized, due to the high temperatures required. Metals such as aluminum and magnesium alloys cannot be boronized because of their low melting points, copper does not form a stable boride [9]. Boronizing the surface of a metal alloy increases the hardness because the crystal structure of boron is more uniform than titanium, which provides a strong protective coating.

Table 3.1 Microhardness and Constitution of Boride Layers on Various Substrates Formed After Boriding [9]

Substrate	Borides constituting layer	Microhardness of layer, kg/mm2
Fe	FeB	1900-2100
	Fe_2B	1800-2000
Co	CoB	1850
	Co_2B	~1550
Co-27.5Cr	CoB	2200 (100g)
	Co_2B	~1550 (100g)
	Ni_4B_3	1600
Ni	Ni_2B	1500
	Ni_3B	900
Inco 100		1700 (200g)
	W_2B	
W	WB	~2700 (overall hardness)
	W_2B_5	
Nb	Nb_2B_4	2600-3000 (overall hardness)
	NbB_4	
Zr	Zr_2B	2300-2600 (overall hardness)
	ZrB_2	
Ta	Ta_2B	3200-3500
Ti	TiB_2	2500 (100g) (overall hardness)
	TiB	
Ti-6Al-4V	TiB_2	3000 (100g) (overall hardness)
	TiB	
Mo	Mo_2B	2400-2700 (overall hardness)
	Mo_2B_5	
Re	ReB	2700-2900

High surface hardness and a low coefficient of friction make boriding an attractive application for use in wear resistance, adhesion, abrasion, and surface fatigue [24]. The microhardness of boronized titanium was studied by Elias Jelis and Figure 3.1 shows the results.

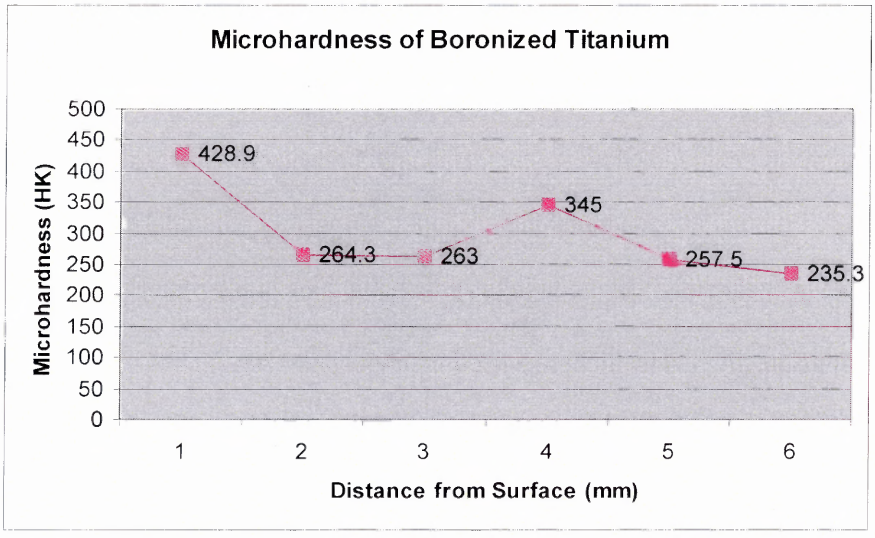

Figure 3.1 Graph of microhardness for boronized titanium [7].

3.2 Mechanism for Boronization

The main driving force behind boronizing is diffusion. During boronizing, the boron atoms migrate into the lattice of the metal substrate, forming an interstitial boron compound with either a single-phase or a multi-phase boride layer. The boronizing process has two distinct steps which both occur during the diffusion of the boron atoms into the metal substrate.

During the first step of boronization, the nuclei of the future boride layer are formed as a function of time and temperature. Once the nuclei have formed, the boride layer begins to grow. The type of metal boride that is formed depends alloy components present. If the boron medium is in excess, the boride layer may contain two or more

intermetallics, in the case of Ti-6Al-4V, titanium boride (TiB) and titanium diboride (TiB_2) are found [24].

The second step is a diffusion-controlled process where the thickness of the boride layer is dependent on both time and temperature according to the parabolic time law:

$$x^2 = kt$$

where x is the thickness of the boride layer, k is a constant depending on the boronizing temperature and t is the boronizing time [11]. The boride layer thickness varies exponentially with temperature, and with time where it shows a parabolic behavior [24]. Figure 3.2 shows a cross-sectional view of the boron layer diffused into the Ti-6Al-4V alloy.

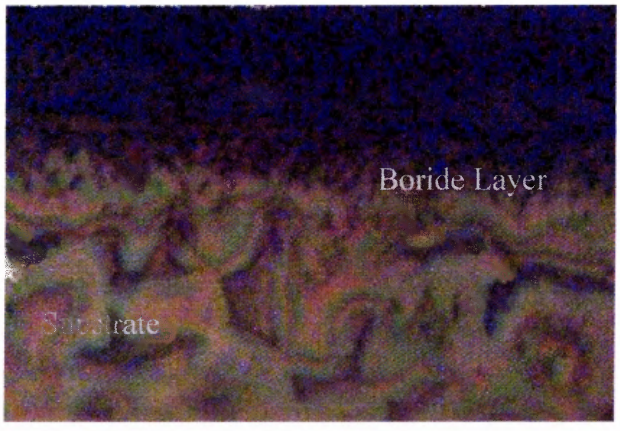

Figure 3.2 Cross-Sectional View of Boron Titanium Sample.

3.3 Boronizing of Nonferrous Metals

Nonferrous metals are metals that contain no iron or very small percentages of iron. Examples of nonferrous metals are aluminum, copper, zinc, titanium, and nickel [4]. Conventional pack boriding and paste techniques are unsuitable for boronizing titanium

because they can cause oxidation of the substrate surface which can lead to corrosion; both contribute to insufficient diffuse of boron into the titanium substrate causing the boride layer to flake off [9]. The oxidation of the titanium layer is a result of an oxygenated atmosphere. Thus, pack boriding in an oxygen free environment, such as in a vacuum with an argon atmosphere, or gas boriding with H_2-BCl_3 gas mixtures, is ideal for boriding titanium without corrosion and oxidation [9].

Boronization for refractory metals and titanium for thickness of 50μm requires processing temperature to be greater than 1000°C for 10 to 15 hours [9]. The microhardness values for titanium and refractory metals are greater than those formed on nickel and cobalt (Table 3.1). The addition of alloys to nickel, cobalt, and titanium retards the rate of boride layer growth and, in the case of titanium; the proportion of multiphased layers (TiB_2) increases as well [9].

3.4 Boronizing Procedure

3.4.1 Pack Boronizing

Pack boronizing is widely used because of the relative safety and simplicity of the process. The metal substrate is imbedded into a boriding powder and placed in a steel or alumina container. The powder is packed down to assure that the powder completely surrounds the metal surfaces. The packed container is placed into a furnace and heated to accelerate the diffusion of boron atoms.

The main boron source in the powder is from boron carbide (B_4C). Also included in the powder are inert diluents such as silicon carbide (SiC) or aluminum oxide (Al_2O_3). These compounds do not aid in the diffusion of boron atoms but rather thin the powder.

Potassium fluroborate (KBF_4) is an activator, which enhances the diffusion of boron carbide because it has strong interatomic bonding and crystalline phases that stabilize the titanium at high temperature.

3.4.2 Paste Boronizing

Paste boronizing is used when pack boronization is not feasible for the application. Paste boronizing is ideal for applications requiring only a portion of the material to be boronized. For example, the femoral head of an artificial hip implant is more likely to undergo wear corrosion, than the implanted stem. Pastes are primarily made of a B_4C suspension and cryolite such as (Na_3AlF_6) or a conventional pack boriding powder mixed in an organic binder.

The application of the paste is usually brushed or sprayed onto the metal; and allowed to dry before another application. The thickness of the paste layer is 1-2mm thick. Once the desired thickness is obtained, the metal is heated in a protective atmosphere such as argon or a vacuum to prevent oxidation.

3.4.3 Liquid Boronizing

Liquid boronizing is also known as salt bath boronizing. There are two techniques used in liquid boronizing: electroless and electrolytic, each is executed at temperatures above 900° C. Since both techniques require the use of salt baths there are restrictions on the size and shape of the materials used (must conform to bath dimensions). Any material placed into the bath must withstand thermal shock upon immersion and removal from the bath otherwise cracking may occur.

Operation and maintenance costs are high with liquid boronizing, because the salt baths require the salt to be recharged. The safety and health risks are also high because both techniques produce corrosive fumes, hydrochloric (HCl) and hydrofluoric (HF_4) fumes.

Electroless salt bath boriding: This treatment requires the reduction of molten borax ($Na_2B_4O_7$). The product of reduced molten borax is a viscous liquid. To help with heat and mass transfer and reduce viscosity of the molten borax the temperature of the bath must range from 900-950°C. Silicon carbide that is commonly used in electroless salt bath coating, is not used in electroless salt bath boriding because it increases the viscosity of the bath water and inhibits the transfer of boron.

Electrolytic boriding: Electrolytic boriding consists of a graphite construction and contains molten borax. The metal substrate is attached to the cathode and the anode is made up of graphite. Both the cathode and anode are immersed in molten borax while a current is applied. The molten borax coats the surface of the metal sample, boron atoms diffuse into the metal substrate forming a boride layer.

3.4.4 Gas Boronizing

Gas boronizing is driven by the thermal decomposition of diborane (B_2H_6). The process can also be based on the reduction of a boron halide, usually BCl_3 with hydrogen. However, diborane is not commonly used in commercial applications because of its toxic and explosive behavior. Boron chloride (BCl_3) is the most attractive of the halogens because boron bromide (BBr_3) can be extremely costly. Also, boron bromide is explosive upon contact with water and is difficult to handle. Boron fluoride (BF_3) is the

most stable, and requires high reduction temperatures. A potential hazardous by-product of gas boriding using boron fluoride, is hydrofluoric fumes (HF).

3.4.5 Plasma Boronizing

The mechanism of plasma boriding involves having high heated materials sprayed onto a host metal surface. The boron powder passes through several heating processes and combines with argon and hydrogen. The heated gas is accelerated in a pressurized chamber (300 Pa to 1500 Pa) and collected into a treatment chamber. The heated gases (700°C to 900°C) are converted into plasma as they travel through the nozzle. The sprayed plasma is then cooled, and sodium hydroxide is washed onto the surface to remove any remaining boron ions. Plasma phase boronizing is not commonly used because of the highly toxic and explosive nature of the boron medium used, boron chloride (BCl_3) and diborane (B_2H_6).

3.4.6 Fluidized Bed Boronizing

The advantage of fluidized bed boronizing is the high rate of mass and heat transfer. This is a benefit because it results in a uniform temperature throughout the volume of the reactor and a flash mix of all compounds contained in it, thus yielding high quality coatings. The downside of fluidized bed boronizing is the poor adhesion of the coating and the uniformity of the boride coating is lacking.

3.4.7 Multicomponent Boronizing

Mutlticomponent boronizing is more of a terminology than a process. Multicomponent boronizing describes the techniques involving the diffusion of boron and one or more metallic element(s) into the surface and near surface regions of the metal substrate [9].

Multicomponent boriding can be carried out in simultaneous or consecutive processing steps:

Type 1: Simultaneous boriding and metallizing (diffusion of the metallic species)

Type 2: Boriding followed by metallizing

Type 3: Metallizing followed by boriding

Table 3.2 Multicomponent Boronizing [9]

Multicomponent boriding technique	**Media type**	**Media composition(s), Wt-%**	**Process steps investigated ***	**Substrate(s) treated**	**Temperature, C**
Boroaluminizing	Electrolytic salt bath	3-20% Al_20_3 in borax	S	Plain carbon steels	900
Boroaluminizing	Pack	(A) 84% B_4C + 16% borax	S	Plain carbon	1050
		(B) 97% ferroaluminium + 3% NH_4Cl	B-Al Al-B	steels	
Borochromizing	Pack	(A) 5% B_4C + 5% KBF_4 + 90% SiC (Ekabor II)	S B-Cr	Plain carbon steels	Boride at 900 Chromized at 1000
		(B) 78% ferrocrome + 20% Al_2O_3 + 2% NH_4Cl	Cr-B		
Borosiliconing	Pack	(A) 5% B_4C + 5% KBF_4 + 90% SiC (Ekabor II)	B-Si Si-B	0.4% C steel	900-1000
		(B) 100% Si			
Borovandium	Pack	(A) 5% B_4C + 5% KBF_4 + 90% SiC (Ekabor II)	B-V	1.0% C steel	Boride at 900 Vanadized at 1000
		(B) 60% ferrovanadium + 37% Al_2O_3 + 3% NH_4Cl			

* S = simultaneous boriding and metallizing.
B-Si borided and then siliconized
Al-B aluminized and then borided.

3.5 Advantages and Limitations of Boronizing

Advantages:

- Boriding of metals by diffusion produces high surface hardness, which can be retained at high temperatures.
- Boronized surfaces are resistant to attacks by molten metals and have moderate oxidation resistance (up to 850°C).
- Boride coatings can be applied to a number of different metals and metal alloys.
- Borided metals have increased fatigue life and service performance under oxidizing and corrosive environments. This is a result of the high hardness of boride and the resistance to oxidation.
- Boriding of titanium alloy improves the microhardness as well improves the corrosion resistance, and prevents pitting corrosion.

Limitations:

- The long processing time causes the process to be less cost effective than other thermochemical coating techniques.
- The thickness of the boride layer depends on the composition of the metal substrate and consistency of the powder mixture.
- Any refinements must be done with a diamond tipped blade because grinding can cause fractures of the boride layers.
- Presence of oxygen during pack boronization can cause oxidation of titanium alloy surface inhibiting the diffusion of boron atoms into the titanium alloy.

CHAPTER 4

HYDROXYAPATITE and BONE

4.1 Structure of Hydroxyapatite

Hydroxyapatite is made up of a calcium phosphate which has been used in the form of artifical bone. Hydroxyapatite has been synthesized and used for implants as well as solids and porous coatings on implants. Depending on the calcium phosphorous ratio, presence of water, impurities, and temperature, calcium phosphate can be crystallized into salts, hydroxyapatite, or β-whitlockite [18]. In a wet environment and at lower temperatures (less than 900°C), hydroxyapatite is more likely to form. Hydroxyapatite is more closely related to the mineral phase of bone and teeth in implant applications than β-whitlockite, it is made of a crystalline form of calcium phosphate similar to hydroxyapatite [$Ca(PO_4)_6(OH)_2$] [18]. The ideal calcium phosphate (Ca/P) ratio of hydroxyapatite is 5:3 and the calculated density is 3.219 g/cm^3 [18].

4.2 Properties of Hydroxyapatite

Hydroxyapatite has a low fracture strength than bone which limits the applications in which hydroxyapatite can be used, hydroxyapatite can not be used exclusively as a bone substitute. However, hydroxyapatite has shown good fixation to the host bone and results in increased host bone growth into the implant. Hydroxyapatite has a high biocompatibility because of the biochemical similarity between the artificial hydroxyapatite and bone and teeth.

4.3 Manufacturing of Hydroxyapatite

The most common application of hydroxyapatite onto a substrate is through a plasma-spray process. In the plasma-spray technique, heated calcium phosphate particles are projected at high velocity in a gas stream onto the metal substrate to build up the coating layer [22]. The ideal hydroxyapatite coating thickness is between 50-75μm thick, which provides better strength than thicker coating layers, because the coating becomes more brittle as the thickness increases over 75μm [22]. The hydroxyapatite coating attaches by mechanical interlocking generated by the energy created by the impact between the hydroxyapatite particles being sprayed and the metal substrate [22]. For ideal performance of hydroxyapatite coatings, the coating should have low porosity, high cohesive strength, good adhesion, moderate-to-high crystallinity, and high chemical and phase stability.

4.4 Structure of Bone

The major load bearing bones of the human skeleton are made up of two types of bone: cortical and cancellous bone. Cortical bone is the stronger of the two bones, and the main factor in the overall strength of a given bone in the skeleton. However, in prosthesis implantation, such as hip implantation, the implant is predominately surrounded by cancellous bone [15].

Cortical bone draws strength from the fact that it is macroscopically a uniform solid, whereas cancellous bone is macroscopically a non-uniform, 3-dimensional array of bony trabeculae with intercommunicating spaces containing bone marrow between the trabeculae [15].

CHAPTER 5

CORROSION

5.1 Definition of Corrosion

Corrosion is the destructive result of a chemical reaction between a metal or metal alloy and its environment [23].

5.2 Mechanism of Corrosion

Nearly all metallic corrosion processes involve transfer of electron charge in an aqueous solution [23]. An example of an electrochemical reaction between zinc and hydrochloric acid is outlined below:

$$Zn + 2HCl \rightarrow ZnCl_2 + H_2 \quad (5.1)$$

In reaction (5.1) the zinc reacts with the hydrochloric acid, which in turn forms zinc-chloride and hydrogen. The same reaction can also be written in the ionic form.

$$Zn + 2H^+ + 2Cl^- \rightarrow Zn^{2+} + 2Cl^- + H_2 \quad (5.2)$$

Because chlorine appears on both sides of the equation in the same quantities it can be removed from the reaction yielding:

$$Zn \rightarrow Zn^{2+} + 2e^- \text{ anodic reaction} \quad (5.3)$$

$$2H^+ + 2e^- \rightarrow H_2 \text{ cathodic reaction} \quad (5.4)$$

The anodic reaction is also known as the oxidation reaction. The oxidation reaction is defined because the zinc loses electrons which can be seen with the increase of the valence from 0 to +2. The opposite can be seen with the cathodic reaction. The cathodic reaction is a gain of electrons, and much like the anodic reaction, the reduction of

hydrogen can also be seen in the equation. The oxidation state of the hydrogen decreases from +1 to 0.

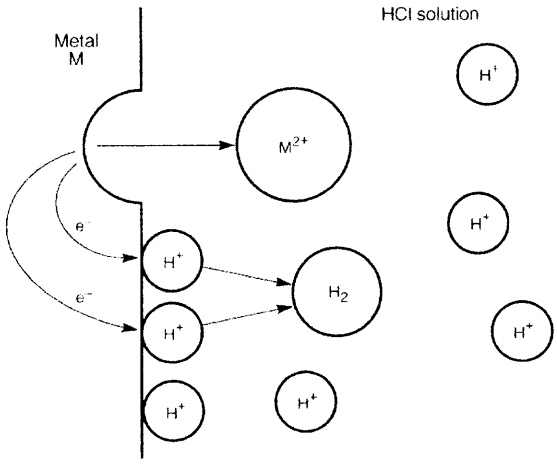

Figure 5.1 Diagram of corrosion system

Figure 5.1 shows the corrosion mechanism of a metal (M) in a hydrochloric acid solution. The unbonded hydrogen atoms remove the valence electrons from the metal substrate. The removal of the metal electrons causes the positive metal atom to leave the bulk and move into the hydrochloric acid solution. This process continues until the metal substrate is completely oxidized.

5.3 Types of Corrosion

There are different types of corrosion causing material to fail in different modes. Some of the most common types of corrosion are list below:

5.3.1 Uniform Corrosion

Uniform corrosion is classified as total and equal corrosion of the metal substrate. Corrosion occurs evenly over the whole surface of the material. In order for uniform corrosion to occur the total surface of the material must be open to the environment.

Uniform corrosion is preferred over many other types of corrosion because the degradation can be easily predicted [23].

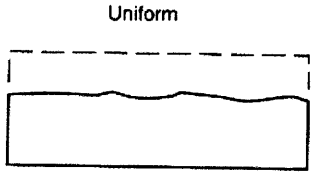

Figure 5.2 Diagram of uniform corrosion [23].

5.3.2 Galvanic Corrosion

Galvanic corrosion occurs between two dissimilar metals coupled together in an electrolyte. Any two metals that have different corrosion potentials will result in galvanic corrosion. Any alloy will corrode when coupled with another alloy that has more noble (positive) potential in the galvanic series. The more noble metal is protected from corrosion while the active (negative) metal corrodes [23].

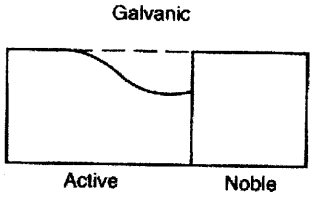

Figure 5.3 Diagram of galvanic corrosion [23].

Table 5.1 Galvanic Series [23]

Cathodic (noble)
platinum
gold
graphite
titanium
silver
zirconium
AISI Type 316, 317 stainless steels (passive)
AISI Type 304 stainless steel (passive)
AISI Type 430 stainless steel (passive)
nickel (passive)
copper-nickel (70-30)
bronzes
copper
brasses
nickel (active)
naval brass
tin
lead
AISI Type 316, 317 stainless steels (active)
AISI Type 304 stainless steel (active)
cast iron
steel or iron
aluminum alloy 2024
cadmium
aluminum alloy 1100
zinc
magnesium and magnesium alloy
Anodic (active)

The more noble (Cathodic) a metal is the more corrosion resistant; the metal alloy is more stable because the need to transfer electrons is minimal. However, the more active (Anodic) the less corrosion resistant the metal behaves. Active metals are unstable because their outer electron shells are incomplete.

5.3.3 Crevice Corrosion

The corrosion of the metal occurs in a crevice or in a sheltered region between two parts, much like that of a bolt and fastener. Crevice corrosion can occur between a metal and nonmetal and is sometimes referred to as deposit corrosion. If the corrosion potentials between the two metals or nonmetals are different, crevice corrosion can be compounded with galvanic corrosion. Crevice occurs when water is retained within the crevice while the outside remains dry [23].

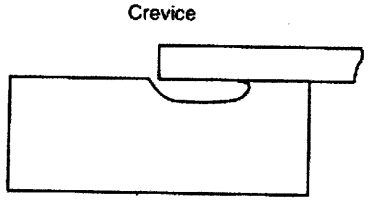

Figure 5.4 Diagram of crevice corrosion [23].

5.3.4 Pitting Corrosion

Pitting corrosion is a localized attack on an otherwise corrosion resistant surface. The localized attacks for pits can be of varying depth (deep, shallow, or undercut). Many metals, such as stainless steels and chromium, depend on a protective passive film to protect the metal from corrosion. However, over time, the passive layer can breakdown in local areas, which allows for the localized attack [23].

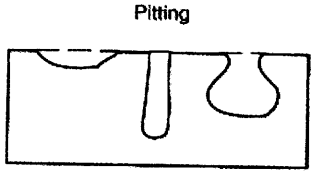

Figure 5.5 Diagram of pitting corrosion [23].

5.3.5 Environmentally Induced Cracking

A normally ductile alloy in the presence of an environment that causes minimal uniform corrosion is known as environmentally induced cracking (EIC). Environmentally induced cracking can be classified into three distinct groupings: stress-corrosion cracking, corrosion-fatigue cracking, and hydrogen-induced cracking.

When an alloy is placed under a static tensile stress while in a specific environmental condition, stress-corrosion cracking occurs. Corrosion-fatigue cracking is much like stress-corrosion cracking; however, the metal is not placed under a static tensile loading but placed under cyclic stresses in a corrosive environment. Both alloys and metals in their pure forms are susceptible to corrosion-fatigue cracking. Hydrogen-induced cracking is caused by hydrogen diffusion into the alloy lattice when the hydrogen evolution reaction produces atomic hydrogen at the surface [23].

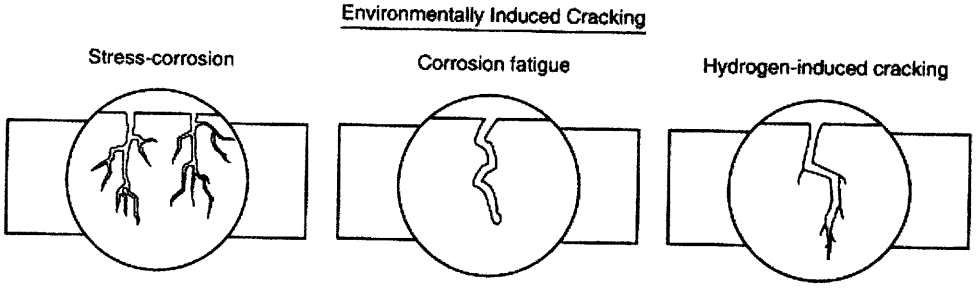

Figure 5.6 Diagram of environmentally induced cracking [23].

5.3.6 Intergranular Corrosion

Intergranular corrosion occurs mostly in alloys, when one of the metal elements such as chromium becomes depleted at the grain boundaries, those grain boundaries become more susceptible to corrosive attack. Intergranular corrosion happens as a result of welding, one of the metal elements in an alloy may have a lower melting temperature than the other elements this melting and vacating the grain boundary [23].

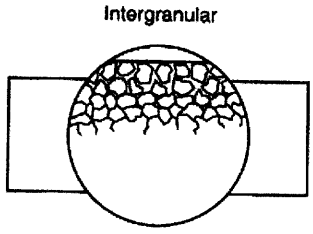

Figure 5.7 Diagram of intergranular corrosion [23].

5.3.7 Dealloying and Dezincification

Dealloying occurs when a metal alloy, such a brass, contains two very different galvanic series characteristics. In brass zinc is much more active (anodic) than copper, which is in the median of the galvanic series in Table 5.1; because of this the zinc leaches out of the brass leaving only the porous copper [23].

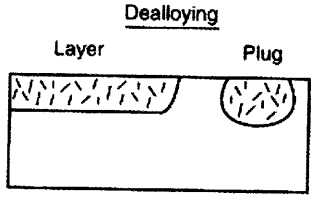

Figure 5.8 Diagram of dealloying corrosion [23].

5.3.8 Erosion-Corrosion and Fretting

Erosion corrosion is caused by both corrosive fluids as well as high flow velocity. Both the corrosive fluids and high velocity fluids remove the protective passive layer of the metal exposing the metal substrate. Once the passive layer is removed, the corrosion process is accelerated [23].

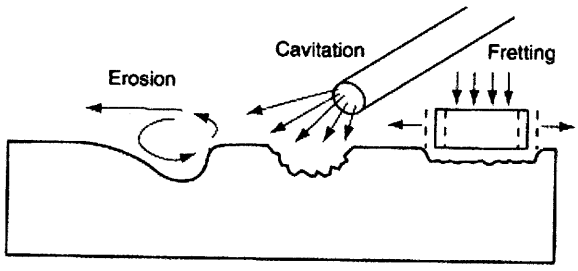

Figure 5.9 Diagram of erosion, cavitation, and fretting corrosion [23].

5.4 Electrochemical Corrosion Methods

5.4.1 Tafel Plots

Most metal corrosion occurs through electrochemical reactions that occur at the interface between the metal and an electrolyte solution. Corrosion normally takes place at a rate determined by an equilibrium between opposing chemical reactions (see Section 5.2). The first of these reactions is the anodic reaction, where a metal is oxidized; this occurs when the electrolyte solution releases electrons into the metal. The other reaction is the cathodic reaction, where the electrolyte solution is reduced by removing electrons from the metal. When both of these reactions are in equilibrium, the flow of electrons back and forth between the two mediums is equal, thus no current flow [43].

A Tafel plot has two axis, where the vertical axis represents the potential and the horizontal axis represents the logarithm of absolute current. The theoretical current or Tafel Constants (β_a and β_c) for both the cathodic and anodic reactions are measured by calculating the tangent of the curved lines as shown in Figure 5.9.

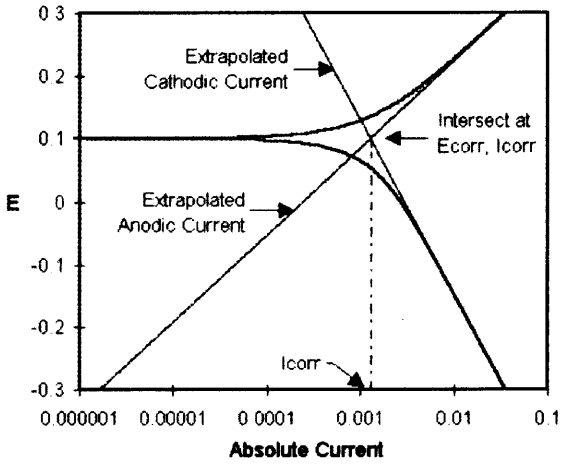

Figure 5.10 Tafel plot diagram [43].

The curved lines in Figure 5.9 represents the total current of the system, or the summation of the cathodic and anodic currents, which occur at the surface of the metal sample. The curved line is the current that is recorded when the potentiostat sweeps the potential of the metal. The horizontal portion of the graph seen at low currents is the point where the current changes signs as the reaction changes from anodic to cathodic. When the potentiostat measures the electrical current before a current is applied to the system is known as Open Circuit Potential (E_{corr}). The point where the two Tafel constants intersect is where E_{corr} is located, and if a vertical line was drawn down from E_{corr} the value for corrosion current (i_{corr}) can be found. When a current is applied to the system and the potential is forced away from the Open circuit potential, the response is used to plot the corrosion behavior of the metal [43].

5.4.2 Linear Polarization Plots

This technique is used to measure the Polarization Resistance (R_p) of a corrosive system. Polarization resistance is defined as the resistance of the specimen to oxidation during the application of an external potential. The corrosion rate is directly related to the R_p and

then can be calculated. The R_p value can be determined by calculating the slope of the linear region of the plot [26,41,42].

To calculate the corrosion rate the corrosion current (i_{corr}) is needed as well as the Tafel Costants (the slopes of the anodic and cathodic regions). The R_p value can help you assess the relative ability of the material to resist corrosion. It is easy to use resistance polarization to assess the corrosion resistance of a material and thus rank materials based on each polarization resistance, as long as all the materials have the same area exposed to the same corrosive environment. The material with the lowest corrosion current or highest R_p value is the most corrosive resistant [41,42].

5.4.3 Passive Layer Formation by Open Cell Potential Measurements

Understanding the formation of a passive layer is important in understanding the kinetics of corrosion. A passive layer is formed on the surface of an exposed metal in a corrosive environment. This passive layer is a thin film of deposited oxide that occurs during corrosion. An example of a passive layer is rust on an iron pipe. A passive layer offers protection to the metal substrate below, slowing the overall corrosion process.

By placing a polished, untested titanium sample into the flat cell and measuring the open cell potential versus time, the time of formation for a passive layer can be plotted. The passive layer formation is measured by the potentiostat by first applying a determined current to the working electrode, the potentiostat then measures the change in current and voltage as a result of passing through the metal sample. The potentiostat applies a different frequency current every two seconds for a pre-determined time set by the user.

5.4.4 Corrosion Rate Calculation

Performing both Tafel and linear polarization experiments are important for the calculation of a samples corrosion rate. Corrosion current, i_{corr}, is used to calculate the corrosion rate of a metal. Most importantly, i_{corr} and corrosion rate are a function of many variables within a system such as metal type, solution composition, temperature, solution dynamics, and metal processing [25].

In order to find the value of i_{corr} a calculation must be made using the following equation:

$$R_p = \beta_a \times \beta_c / [2.3 \times i_{corr} \times (\beta_a \times \beta_c)]$$

By rearranging the above equation to solve for i_{corr} (A/cm^2), we obtain the following equation for i_{corr}.

$$i_{corr} = \beta_a \times \beta_c / [2.3 \times R_p \times (\beta_a \times \beta_c)]$$

Another calculation must be determined before the samples corrosion rate can be found and that is the samples equivalent weight (E.W.). The equivalent weight is found from the equation:

$$N_{eq} = \Sigma(f_i \times n_i / a_i)$$

where,

f_i is the mass fraction of each element present in the metal compound

n_i is the number of electrons in the outer shell also known as valency

a_i is the atomic weight of the alloying element in grams

Equivalent weight is the reciprocal of N_{eq} thus making the equation for equivalent weight:

$$E.W. = 1/ N_{eq}$$

Once, i_{corr} and equivalent weight (E.W.) are calculated, the samples corrosion rate can be calculated in milli-inches per year (MPY).

$$\text{Corrosion Rate (MPY)} = (0.13 \times i_{corr} \times \text{E.W.}) / (A \times D)$$

A is the cross-sectional area of the exposed sample to the corrosion solution (cm^2)

D is the density of the sample (g/cm^3)

CHAPTER 6

ELECTROCHEMICAL IMPEDANCE SPECTROSCOPY

6.1 Overview of Electrochemical Impedance Spectroscopy

Electrochemical impedance spectroscopy (EIS) is a technique used to produce accurate, kinetic, and mechanistic information of a material [41,42]. Some of the applications that EIS can be used for are listed in the table below:

Table 6.1 Applications for EIS [41,42]

RESEARCH AREA	APPLICATION
Corrosion	Rate Determinations Inhibitor and Coatings Passive Layer Investigations
Coatings Evaluation	Dielectric measurements Corrosion Protection
Batteries	State-of-charge Materials Selection Electrode Design
Electrodeposition	Bath Formulation Surface Pretreatment Deposition Mechanism Deposit Characterization
Electro-Organic Synthesis	Adsorption/Deposition Reaction Mechanism
Semiconductors	Photovoltaic work Dopant Distributions

EIS uses relatively small excitation amplitudes, commonly ranging from 5 to 10mV peak-to-peak. These small excitation amplitudes decrease the perturbation of the electrochemical test system, thus reducing the errors of the technique. EIS measures two parameters of a material, capacitance and charge-transfer kinetics. Data collected from both of these areas provides important mechanistic information. Finally, EIS does not require a potential scan and as a result measurements can be collected using a low

conductivity solution [41,42]. Electrochemical impedance spectroscopy is dependent on modification of the current through the sample metal. Impedance is closely related to resistance such that they both oppose the flow of electrons or current. In direct current (DC current) circuits, electron flow or current is impeded only by resistors. In alternating current (AC current) circuits, electron flow is impeded by capacitors and inductors. Impedance itself can be expressed as a complex number, that is, it can be separated into two parts: real and imaginary. The resistance represents the real portion and the imaginary portion is represented by a combination of both the capacitance and inductance.

Capacitors and inductors affect the magnitude (strength) of the alternating current as well as the time dependent characteristics or phase. When a current is placed across an AC circuit and the highest resistance is seen across the capacitor, a circuit is said to be largely capacitance and the current leads the applied voltage in phase angle. If more resistance is seen across the inductor, a circuit is said to be largely inductive and the current lags the applied voltage in phase angle.

6.2 Theory of Electrochemical Impedance Spectroscopy

Electrochemical impedance theory describes the response of a circuit to an alternating current or voltage as a function of frequency. Electrochemical impedance is driven by AC (alternating current) voltage. In basic AC theory the frequency is non-zero and Ohm's law takes on the following form:

$$E = IZ \tag{6.1}$$

Where E and I are defined as potential and current, Z is defined as impedance, which is the equivalent of resistance in DC theory. Impedance values are measured in ohms (Ω) the same as resistance. Impedance is measured by applying a AC potential to an electrochemical cell and measuring the current through the cell. When a sinusoidal potential excitation is applied to the cell, an AC current signal response containing an excitation frequency and it's harmonics are captured. Impedance is measured in resistors, capacitors, and inductors because in an electrochemical cell, slow electrode kinetics, chemical reactions, and diffusion can all impede electron flow much like they do in electrical systems.

A monochromatic excitation signal $E(t) = E_o \cos \omega t$ is applied to a cell and the resulting steady state current $I(t) = I_o \cos (\omega t + \theta)$ measured. The time-dependent current response I(t) of an electrode surface to a sinusoidal alternating potential signal E(t) is expressed as an angular frequency (ω) and dependent impedance Z(ω) where:

$$Z(\omega) = E(t) / I(t) \qquad \text{(Conventional Impedance)} \qquad (6.2)$$

$$E(t) = E_o \cos \omega t \qquad \text{(Excitation Signal)} \qquad (6.3)$$

$$I(t) = I_o \cos (\omega t + \theta) \qquad \text{(Response Signal)} \qquad (6.4)$$

E_o and I_o represent the amplitude of the voltage (E_o) and the current (I_o), ω is the radian frequency. Various processes at the surface of a substrate absorb electrical energy at discrete frequencies, causing a time lag between the time-dependent excitation and response signals. Theta (θ) represents the phase difference between the voltage and the current, Figure 6.1. When θ is equal to zero, the substrate is behaving purely like a resistor.

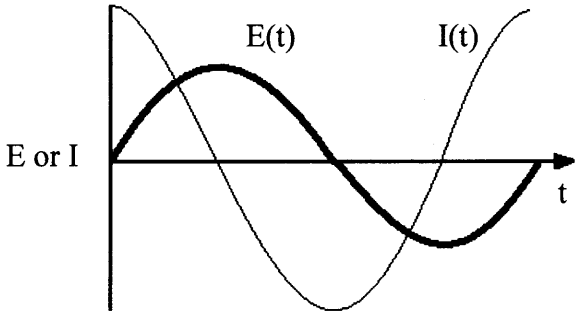

Figure 6.1 Phase lag between excitation signal (E) and response signal (I).

By using Euler's relationship:

$$\text{Exp}(j\theta) = \cos\theta + j\sin\theta \tag{6.5}$$

it is possible to express the impedance as a complex function for potential (E_o) and current (I_o).

$$E(t) = E_o \exp(j\omega t) \tag{6.6}$$

$$I(t) = I_o \exp(j\omega t + j\theta) \tag{6.7}$$

By plugging the potential (E_o) and current (I_o) into Ohm's law, Equation 6.1, the complex function for impedance is found.

$$Z = Z_o(\cos\theta + j\sin\theta) \tag{6.8}$$

Cos θ represents the real portion of the impedance while jsin θ represents the imaginary portion. As a result of time lag, the impedance can be read in two forms: the real (Z') and the imaginary (Z''). The total impedance of the system can be determined by the sum of both the real and imaginary impedance:

$$Z(\omega) = Z'(\omega) + Z''(\omega) \tag{6.9}$$

The real portion of the signal response represents the resistance, while the imaginary represents the capacitance. By plotting the real impedance against the imaginary impedance, a Nyquist plot is formed, Figure 6.2.

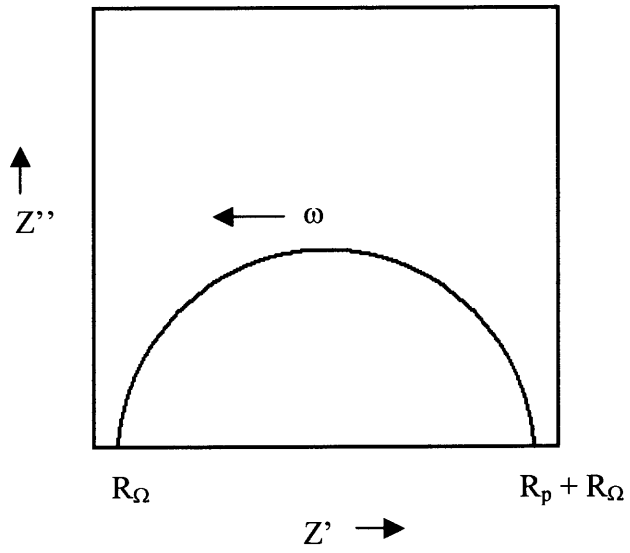

Figure 6.2 Nyquist plot.

The R_Ω value in the Nyquist plot represents the resistance of the conducting solution used. The R_p value represents the polarization resistance of the metal sample. In order to calculate the R_p value the difference of $R_\Omega + R_p$ and R_Ω must be taken:

$$R_p = (R_\Omega + R_p) - R_\Omega$$

However, interpreting data from the Nyquist plot can be difficult because Nyquist plots do not reference the frequency at which the measurement was taken. A Bode plot, Figure 6.3, is able to show frequency, but does so by plotting impedance versus log frequency and plotting phase shift versus log frequency.

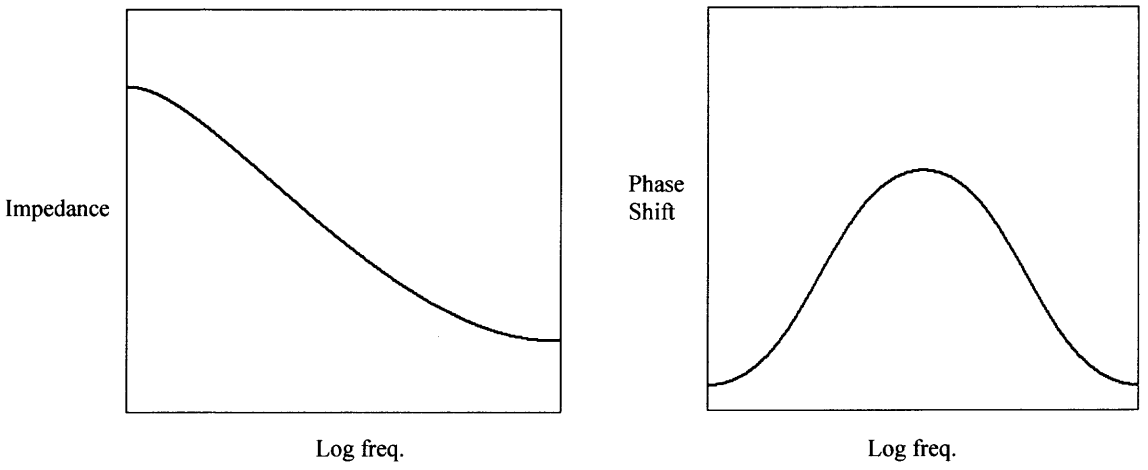

Figure 6.3 Bode plots.

Electrochemical impedance spectroscopy is used to measure metal's impedance to corrosion. By understanding the metals resistance to corrosion under specific environments, a metal can be engineered for that application. EIS testing allows the user to find an equivalent circuit, which represents the corrosion system. Each component of the equivalent circuit is represented by a different component of the system. The resistance of the corrosive solution is represented by R_{Ω}, which is in units of ohms. The resistance of the metal sample is given by R_p and the capacitance of the metal is given by C_{dl} in units of Farady.

6.3 Advantages and Limitations of EIS

Advantages:

- Ability for potential to be automated. Results may be correlated to material variables such as mass transport, rate of chemical reactions, corrosion, and dielectric properties.
- Ability to predict the performance of chemical sensors and investigate membrane behavior in living cells.
- Produce theoretical electrical circuit models that aid in the analysis of material properties.
- Allows for accelerated corrosion testing.

Limitations:

- Difficulty interpreting data plots.
- Confusion in material behavior as a result of theoretical circuit models that can be rearranged and produce the same impedance data.

CHAPTER 7

EXPERIMENTAL PROCEDURE

7.1 Experimental Process

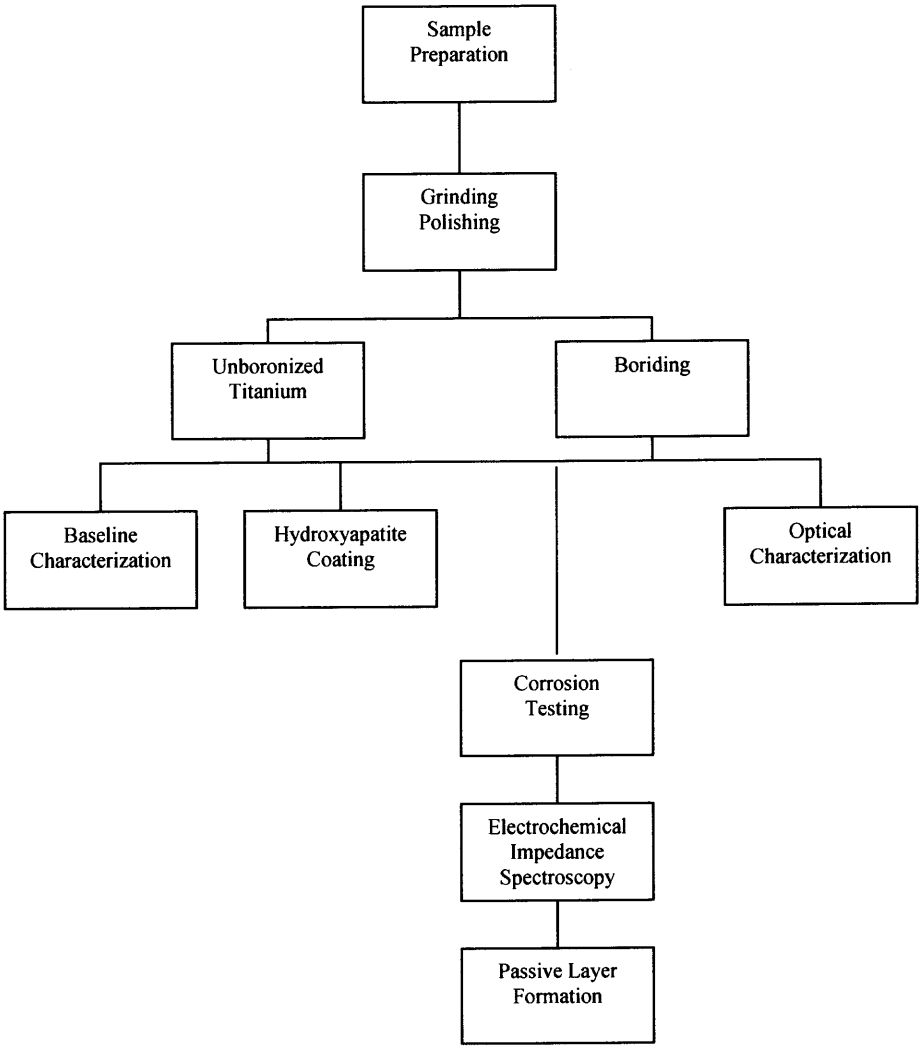

7.2 Boron Treatment Procedure

7.2.1 Sample Preparation

The first step of sample preparation is to cut the titanium alloy into usable samples. The titanium alloy comes in 1" x 1" x 0.25" squares, which are too large to boronize. The samples were cut down to 0.5" x 0.5" x 0.25" squares using a diamond tipped blade. Next, all six surfaces were ground down using silicon carbide sandpaper. The sanding process began with 120-grit sandpaper until all major scratches and burs were removed. The process was continued with 220, 400, and 600-grit sandpaper until all surfaces were uniform. Once the grinding was complete, samples were placed in an ultrasonic bath with cleanser for 1 to 2 minutes and then again with acetone for another 1 to 2 minutes to remove the cleanser residue.

7.2.2 Boron Powder Mixture Preparation

Boronizing was done in a vacuum furnace using a powder cocktail consisting of boron carbide, aluminum oxide, and potassium tetrafluoroborate. The percentages of each ingredient are listed as follows in Table 7.1:

Table 7.1 Percentages of Compounds in Boron Powder

Compound	Percentage	Specifications
Boron Carbide	85-94%	240 grit, technical grade Electro Abrasives Corporation
Aluminum Oxide	5-10%	99.99%, 20-30 micron of Atlantic Equipment Engineers
Potassium Tetrafluoroborate	1-5%	99% min (assay), typically >99.5% (assay) of Alfa Aesar

Aluminum oxide and potassium tetrafluoroborate were weighed to their corresponding ratios. The potassium tetrafluoroborate was placed inside a mortar and pestle along with the aluminum oxide. The two compounds were then mixed until evenly

incorporated; this was done to break up any clusters. Next, the boron carbide was weighed out and was then added to the aluminum oxide/potassium tetrafluoroborate mixture in small increments. The boron carbide was stirred into the mixture with the mortar and pestle to insure even distribution; this helps prevent the segregation of the aluminum oxide from the potassium tetrafluoroborate, the segregation between the two components can cause uneven diffusion of boron into the metal substrate. Once the mortar was filled with powder, the remaining boron carbide powder and mortar mixture were placed into a container with a lip and shaken to insure an even mixture.

7.2.3 Boronizing Process

The boron powder was dried in a box furnace (ThermoLyne model 48015) at 250°C for two hours, and the polished titanium samples were placed next to one another approximately 1 cm apart from one another and approximately 5-10 millimeters from the top of the powder. The remaining dried boron powder was then placed on top of the titanium samples. After the crucible was completely filled, the crucible was tapped to make sure the powder completely surrounded the samples and any voids in the powder were removed.

7.2.4 Heat Treatment of Boron Powder

The filled crucible was placed into a vacuum furnace (ThermoLyne 21100 Tube Furnace) taking extra care to ensure nothing was touching the walls, since crucible heat can cause the glass tube vacuum tube to break. The furnace was sealed and a vacuum pressure of 700 mm Hg was applied. The temperature of the furnace was increased to and maintained at 950°C for four hours. Once the required boronizing temperature and

duration was reached, the samples were allowed to cool under vacuum. Then the boronized samples were removed from the crucible and rinsed with methanol and placed into an ultrasonic bath to remove any residual residue.

7.3 Hydroxyapatite Coating

NaOH treatment: Both polished unboronized and boronized titanium alloy were cleaned in an ultrasonic bath containing isopropyl alcohol for 10 minutes. After the 10 minute wash the isopropyl alcohol was replaced with acetone and placed back in the ultrasonic bath for 15 minutes. Finally, the samples were placed in deionized water for 5 minutes to remove any residual alcohol from the surface. The cleaned samples were then treated in 5 M NaOH solution at 60°C for 24 hours. After, the 24-hour treatment the samples were placed back into deionized water for five minutes.

SCS Solution treatment: The hydroxyapatite coating, also known as supersaturated calcification solution (SCS), was prepared by dissolving 1110 mg $CaCl_2$, 300 mg NaH_2PO_4, and 126 mg of $NaHCO_3$ in deionized water [19]. The NaOH treated samples were placed into a beaker containing 200 ml of SCS solution. The beaker was placed onto a magnetic hot plate set at a temperature of approximately 37°C with a stirring rate of approximately 80 revolutions per minute. The samples were left in the SCS solution for 24-hours before they were removed and washed with deionized water. The samples were then placed in an oven at 60°C for two hours.

7.4 Corrosion Testing

Corrosion testing was carried out using Hank's solution, which is a simulated body fluid containing different salt compounds, urea, glucose, and is buffered at a pH of 7.2. The solution was naturally aerated and all experiments were carried out at room temperature. The experimental procedure is as follows:

- Baseline sample surface image was captured using an optical microscopy at 100x, 250x, and 500x magnification.
- The sample was then placed into the corrosion flat cell and tightened down.
- The reference electrode compartment was filled with Hank's solution. A small amount of Hank's solution was allowed to bleed through the plastic tubing to insure that no air bubbles were present. The reference electrode compartment was again filled with Hank's solution and the Ag-AgCl KCl saturated reference electrode was placed inside.

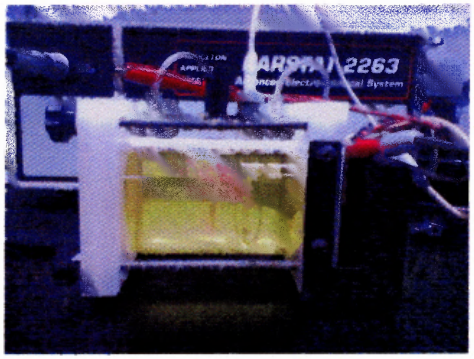

Figure 7.1 Flat cell with Hank's solution.

- The flat cell is filled with approximately 270 ml of Hank's solution.
- Next, a filled stopcock was placed into the flat cell and rubber tubing was placed into the cell for aeration.
- The flat cell was then connected to the potentiostat according to manufacturer's instructions, and then connected to a computer.
- Once all of the connections were made, the PowerSuite (Princeton Applied Research) corrosion software was opened.

- The desired experiment was selected and the test parameters were entered. For the Tafel plot experiment the scan range was set to ±250 mV with respect to the open circuit potential. The scan rate was set for 1 mV/s [33,34,35].

- The open circuit potential experiment was run using the PowerCorr software (Princeton Applied Research) for one hour prior to data collection. During the open circuit experiment, the free currents generated during the exposure of the sample to the corrosive environment were measured with respect to time [25].

- After the instrument had set the open circuit potential, the test began and data were recorded.

- Once the Tafel experiment was complete the Hank's solution was replaced and a linear polarization experiment was conducted.
- The test parameters were set to a scan range of ±0.02mV versus the open circuit potential. The scan rate was set for 0.166 mV/s.

- Once all the data were collected the titanium sample was removed from the flat cell and placed into Hank's solution. The sample and Hank's solution were then placed inside of an incubator set at 37°C for a pre-determined length of time.

7.5 Characterization Methods

7.5.1 Optical Microscopy

Optical microscopy images were taken before each corrosion test to determine if there were any changes to the surface of the sample during degradation. Images were taken with a Pixelink PL-A662 digital camera and Axio Tech optical microscope with a 5x eyepiece and 20x, 50x, and 100x objective lens.

7.5.2 Scanning Electron Microscopy

Scanning Electron Microscopy images were taken using a LEO 1530VP PESEM Scanning Electron Microscope. Scanning electron microscope images were taken of the samples after selected corrosion time points. Scanning electron microscopy is able to magnify the surface of the sample better than optical microscopy methods. Scanning

electron microscopy is also able to determine if the sample is susceptible to pitting corrosion.

7.5.3 Electrochemical Impedance Spectroscopy Testing

EIS testing was carried out on a Princeton Applied Research PotentioStat 2263 series using a standard flat cell with an Ag-AgCl KCl saturated reference electrode. Sample preparation was identical to preparation outlined for Tafel and linear polarization tests. The test parameters were set to scan a frequency between 100kHz to 10 mHz recording 20 points per decade. The scanning frequency was set to an amplitude of 10 mV/s. EIS data was analyzed using ZSimpWin Electrochemical Impedance Software to produce an equivalent circuit.

7.5.4 Open Cell Potential Test

Open cell potential measurements were carried out in a flat cell and followed the same setup as Tafel and linear polarization tests. The open cell potential was set to measure a frequency range of ± 250 mV for a duration of 48 hours. A plot of potential versus time is given.

CHAPTER 8

RESULTS AND DISCUSSION

8.1 Corrosion Testing for Boronized Titanium

Both the boronized and unboronized titanium alloys were tested in naturally aerated Hank's solution for polarization resistance, and Tafel plots.

8.1.1 Boronized Titanium Day 0 (Baseline)

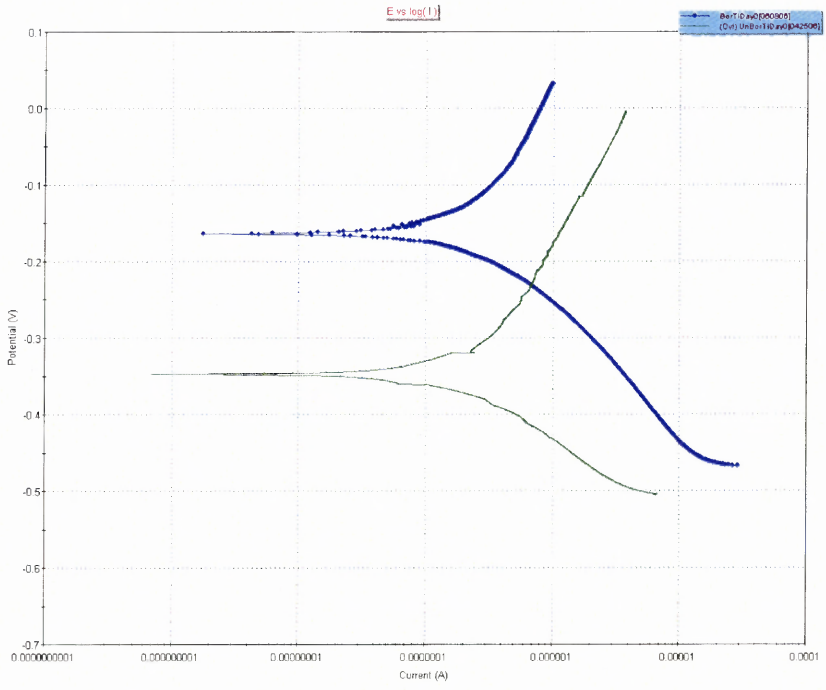

Figure 8.1 Tafel plot at Day 0 (Baseline) for unboronized titanium alloy versus boronized titanium alloy. Boronized titanium alloy is shown in blue, while unboronized titanium alloy is shown in green.

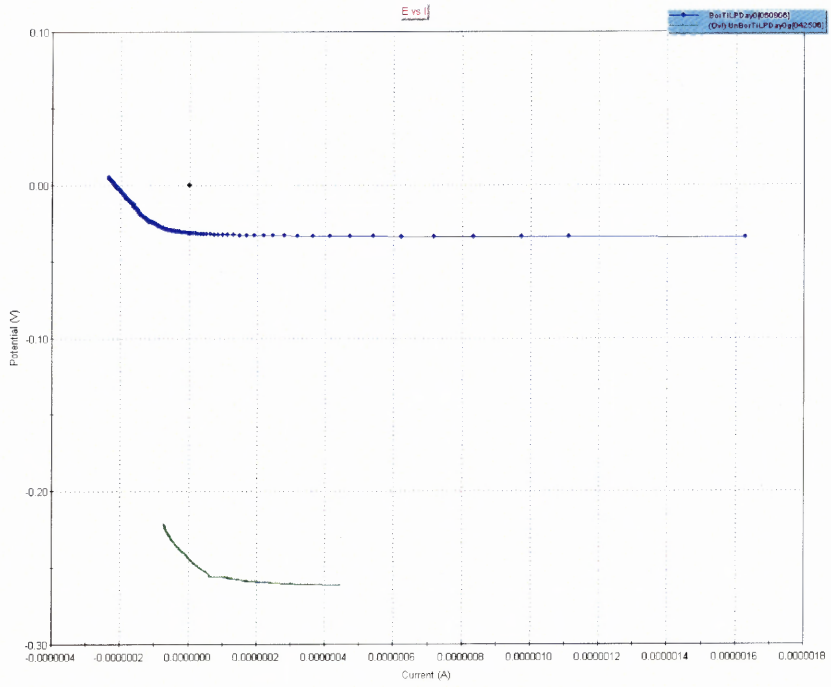

Figure 8.2 Linear polarization plot at Day 0 (Baseline) for unboronized titanium alloy versus boronized titanium alloy. Boronized titanium alloy is shown in blue, while unboronized titanium alloy is shown in green.

The Tafel plot of boronized versus unboronized titanium alloy is shown in Figure 8.1. The E_{corr} value of the boronized titanium alloy (graph in blue) is shown to be approximately –0.16V compared to the –0.35V shown by the unboronized titanium alloy (graph in green). The more positive E_{corr} value of boronized titanium demonstrates that the boronized titanium alloy sample is more corrosion resistant than the unboronized titanium alloy since both boronized and unboronized titanium alloy have the same corrosion current i_{corr} only the corrosion potential can be compared.

The linear polarization plot, Figure 8.2, provides corresponding results as those in the Tafel plot. The resistance polarization (R_p), calculated from the slope shown in Figure 8.2, value for boronized titanium alloy (graph in blue) is much higher than the resistance polarization value for unboronized titanium alloy (graph in green),

demonstrating the boron layer on the titanium alloy is more corrosion resistant than the unboronized titanium alloy, which had no passive layer.

8.1.1.1 Calculations. The first step to calculating corrosion rate is to calculate the equivalent weight for both unboronized and boronized titanium alloy, using the following formulas for equivalent weight:

$$N_{eq} = \Sigma(f_i \times n_i / a_i)$$

$$E.W. = 1/ N_{eq}$$

For unboronized titanium alloy, the composition of each component must be found. Using the chemical composition for the titanium alloy (Ti-6Al-4V) the percentages of each component are known.

Table 8.1 Elemental Composition, Valency, and Atomic Weight of Ti-6Al-4V and Boron

Element	Percentage (f_i)	Valency (n_i)	Atomic Weight (a_i)
Ti	90%	4	47.9
Al	6%	3	26.982
V	4%	5	50.942
B	Not Present in Alloy	3	10.811

Valency represents the number of unoccupied electrons in the elements outer most shell. The valency of each atom can be found by utilizing a periodic table. The group number (number located at the top of each column) indicates the elements valence number. The atomic weight of each element can also be found using a periodic table.

Once all the variables have been found, they can be plugged into the equations found above to yield the alloy's equivalent weight:

$$N_{eq} = 8.58$$

$$E.W. = 11.66$$

Calculating the corrosion rate of the metal first requires the determination of i_{corr}. Since i_{corr} can not be measured accurately from the Tafel plot, i_{corr} must be calculated using the equation for resistance polarization:

$$R_p = \beta_a \times \beta_c / [2.3 \times i_{corr} \times (\beta_a \times \beta_c)]$$

By performing a Tafel plot both β_a and β_c are found. Also, by performing a linear polarization test the value for R_p is found. Solving the equation gives:

$$i_{corr} = 1.5 \times 10^{-4}\ \mu A$$

Finally, by estimating i_{corr}, the equivalent weight, area test, and density of the alloy, the corrosion rate of the sample can be calculated.

$$\text{Corrosion Rate (MPY)} = (0.13 \times i_{corr} \times E.W.) / (A \times D)$$

All variables found the corrosion rate for unboronized titanium at Day 0 to be:

$$\text{Corrosion Rate (MPY)} = 0.000162$$

The same calculations are made for boronized titanium, but the process used to find the equivalent weight is different. Since only the surface of the boronized titanium is in contact with the corrosion environment, only the composition of the titanium diboride layer is needed. However, in the case of boronized titanium alloy, both titanium boride (TiB) and titanium diboride (TiB_2) exist on the surface.

To calculate the equivalent weight of boronized titanium alloy, the composition of titanium and boride present in both titanium boride and titanium diboride must be found.

By using simple percent composition techniques, the composition of each component can be found.

Table 8.2 Atomic Weight and Atoms Present in Compound

Element	Atomic Weight (a)	Atoms
Ti	47.9	1
B	10.811	1
B_2	10.811	2

To find the composition percent for titanium boride, the atom weight of each element must be multiplied by the number of atoms that appear in the surface layer, for titanium boride only one titanium atom and one boron atom exist (TiB):

$$Ti = 1 \times 47.9$$

$$B = 1 \times 10.811$$

The summation of the elemental weight gives the compound's total weight.

$$\Sigma \text{ TiB} = 58.711\text{g}$$

Dividing each elements weight by the total weight yields the percentage of that element in the total compound.

$$Ti = 47.90/58.711$$
$$= 81.59\%$$

$$B = 10.811/58.711$$
$$= 18.41\%$$

The same process is followed for determining the percentage of each element in the titanium diboride compound.

$$Ti = 1 \times 47.90$$

$$B = 2 \times 10.811$$

$$\Sigma TiB_2 = 69.522\text{g}$$

Dividing each elements weight by the total weight of the compound, the percentage of each element is found.

$$Ti = 47.90/69.522$$
$$= 68.9\%$$

$$B_2 = 21.62/69.522$$
$$= 30.96\%$$

Table 8.3 Percentage of Boron and Titanium in Boronized Titanium Alloy

Compound	Density (g/cm^3)	% Boron	% Titanium
TiB	4.48	18.41	81.59
TiB_2	4.52	30.96	68.9
Average	4.5	24.685	75.25

Since the boride layer of the boronized titanium alloy consists of both titanium boride and titanium diboride the averages of both boron and titanium percentages will be used to calculate the equivalent weight.

$$N_{eq} = 13.14$$

$$E.W. = 7.6$$

Calculating the corrosion rate for boronized titanium alloy is identical to unboronized titanium alloy. The i_{corr} value for boronized was calculated to be 2.2×10^{-4}. Following the calculation of i_{corr} the corrosion rate was calculated to produce a corrosion rate of 0.00015 MPY.

Table 8.4 Experimental and Calculated Corrosion Data at Day 0

Day	Sample	β_X	β_A	Rp (Ω)	Icorr (μA)	Corrosion Rate (MPY)	Equivalent Weight (g)	Area (cm^2)	Density (g/cm^3)
0	Unboronized	113.72	305.797	2.5×10^5	1.5×10^{-4}	1.62×10^{-4}	11.66	0.318	4.42
	Boronized	182.805	310.422	2.3×10^5	2.2×10^{-4}	1.5×10^{-4}	7.6	0.318	4.5

Since the corrosion rate is measured in milli-inches per year the difference between the two samples is quite significant.

8.1.1.2 Optical Microscopy. Images of samples taken before corrosion testing and degradation testing in Hank's solution at 37° C.

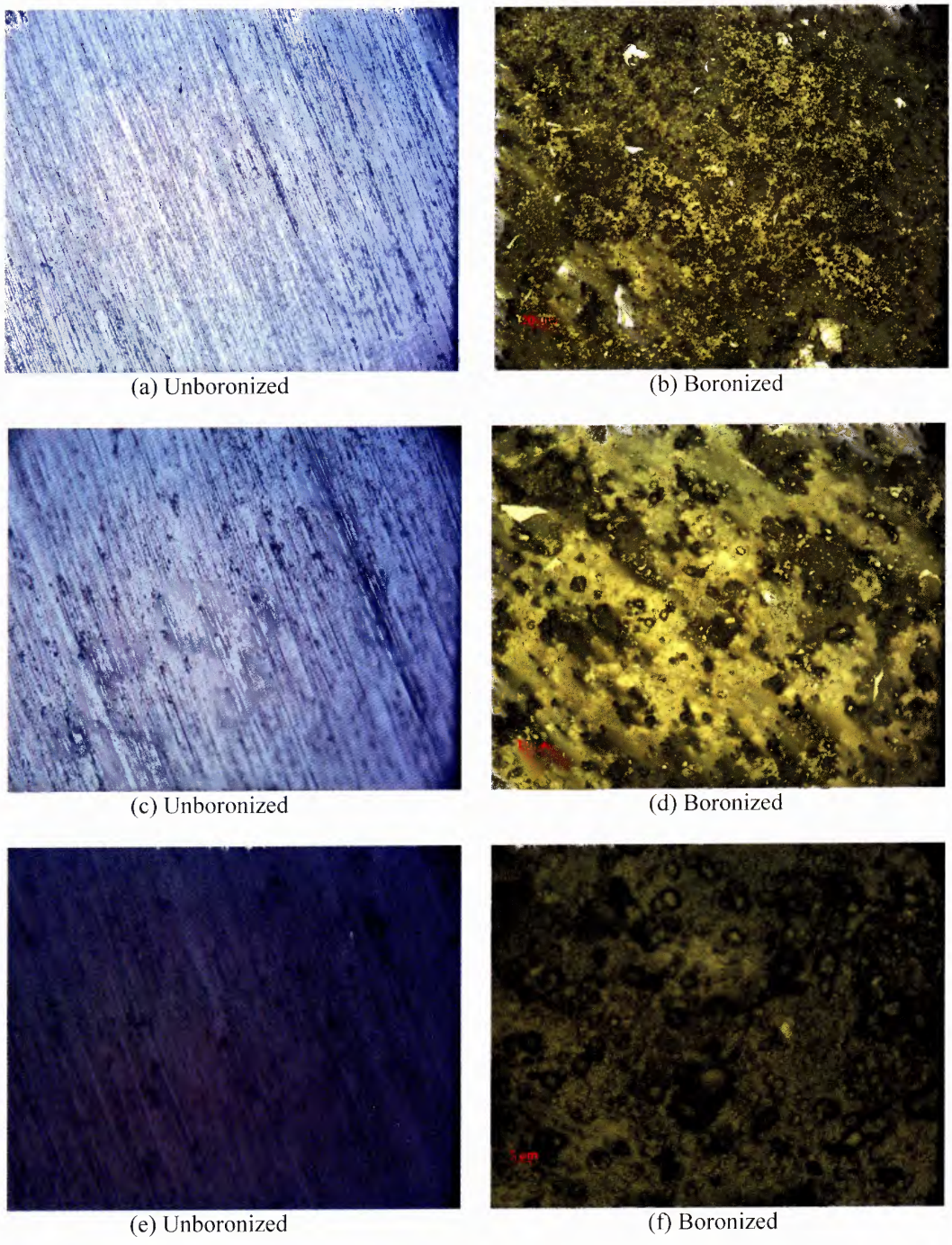

(a) Unboronized (b) Boronized

(c) Unboronized (d) Boronized

(e) Unboronized (f) Boronized

Figure 8.3 Images of titanium alloy samples surfaces at Day 0 (Baseline) prior to corrosion testing in Hank's solution, images (a) and (b) taken at 100x magnification, images (c) and (d) taken at 250x magnification, and images (e) and (f) taken at 500x magnification.

The initial optical images are important because they reference other images taken at different time points during the degradation study. The Day 0 optical images show the surface of both unboronized and boronized titanium alloy prior to corrosion testing. The surface of the unboronized titanium alloy in Figure 8.3 (a,c,e) shows that prior to corrosion testing, there are no pits or surface defects other than the grain markings made from polishing the surface of the titanium alloy.

The optical images of the boronized titanium alloy, Figure 8.3 (b,d,f) indicates the surface of the boronized titanium alloy is not homogeneous. In Figure 8.3 (b) shows areas of polished unboronized titanium alloy, which can be affected by corrosion testing. Optical images taken at 250x and 500x magnification, Figure 8.3 (d,f), show a 3-dimensional boride layer on the surface.

8.1.1.3 Scanning Electron Microscopy.

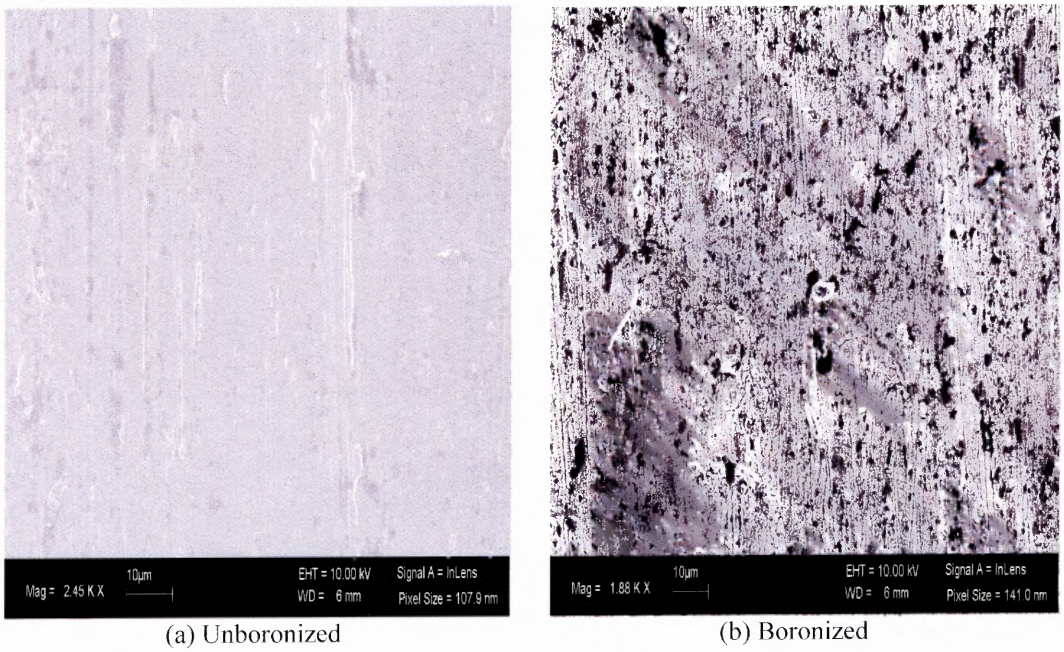

(a) Unboronized (b) Boronized

Figure 8.4 Scanning electron microscope image of unboronized titanium alloy versus boronized titanium alloy at Day 0 (baseline).

The SEM images showed that the unboronized titanium alloy only had grains due to surface polishing. No signs of pitting, crevice, or dealloying corrosion were seen on the surface. The boronized titanium alloy showed areas were grains of boron powder remained, these were the black spots on the surface. Areas where boronization failed to diffuse into the surface were also confirmed.

8.1.2 Boronized Titanium Alloy Day 1

The titanium alloy samples were tested 24 hours after the initial baseline corrosion parameters were measured. After the baseline corrosion testing was concluded, the titanium alloy samples were placed in Hank's solution and then placed into an incubator at a temperature of 37°C. After the 24-hour incubation period, samples were removed and tested. Optical microscopy images were taken as well.

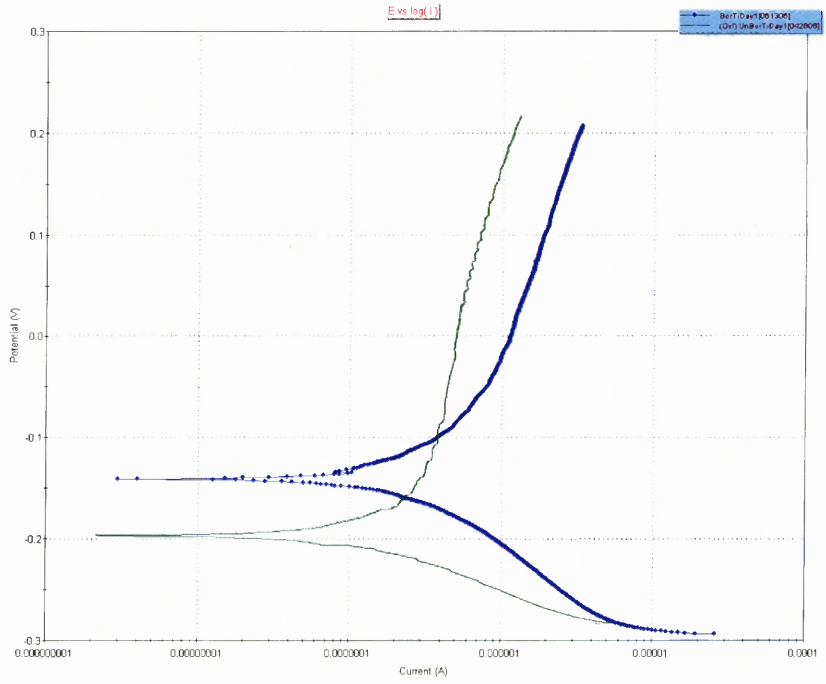

Figure 8.5 Tafel plot at Day 1 for unboronized titanium alloy versus boronized titanium alloy. Boronized titanium alloy is shown in blue, while unboronized titanium alloy is shown in green.

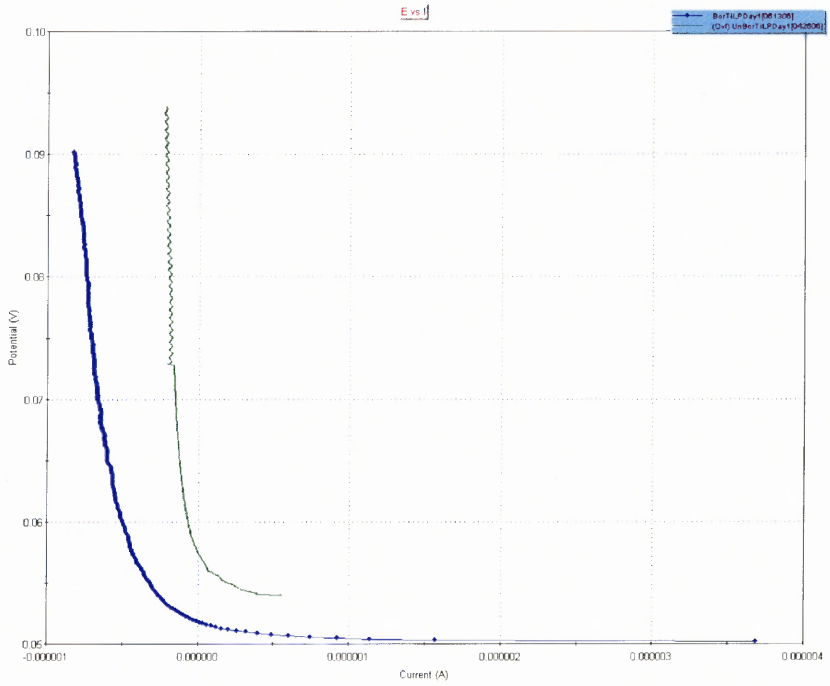

Figure 8.6 Linear polarization plot at Day 1 for unboronized titanium alloy versus boronized titanium alloy. Boronized titanium alloy is shown in blue, while unboronized titanium alloy is shown in green.

Corrosion testing prior to 24 hours of sample incubation in Hank's solution shows different results than in the baseline data shown at Day 0, Figure 8.1. The Tafel plots for boronized titanium alloy show little difference between Day 0 and Day 1. The corrosion potential value does not change significantly; the corrosion potential decreases from –0.16V to –0.14V. The increase in nobility can be attributed to a formation of a titanium dioxide layer forming over the unboronized titanium alloy that still remained after boronizing. Unlike boronized titanium alloy, unboronized titanium alloy had a very significant change between Day 0 and Day 1. Unboronized titanium alloy increased in nobility from –0.35V to –0.19V. The increase in nobility for the unboronized titanium alloy is also a result of a formation of a titanium dioxide passive layer. Titanium dioxide is less conductive thus decreasing the titanium alloy conductivity. The titanium dioxide passive layer forms a protective coating on the surface of the unboronized titanium alloy,

inhibiting corrosion from occurring at the metal surface. However, unlike titanium diboride, titanium dioxide is very weak and wears very easily.

The linear polarization for the unboronized titanium alloy is more corrosion resistant than the boronized titanium alloy, according to Figure 8.6. This increase in corrosion resistance for unboronized titanium alloy is due to the titanium oxide layer on the surface. Titanium oxide is less conductive than titanium boride, thus the thicker the titanium oxide passive layer the higher the resistance polarization.

8.1.2.1 Calculations.

Table 8.5 Experimental and Calculated Corrosion Data at Day 1

Day	Sample	β_X	β_A	Rp (Ω)	Icorr (μA)	Corrosion Rate (MPY)	Equivalent Weight (g)	Area (cm^2)	Density (g/cm^3)
0	Unboronized	113.72	305.797	$2.5x10^5$	$1.5x10^{-4}$	1.62×10^{-4}	11.66	0.318	4.42
	Boronized	182.805	310.422	$2.3x10^5$	$2.2x10^{-4}$	1.5×10^{-4}	7.6	0.318	4.5
1	Unboronized	60.992	642.649	$2.2x10^4$	$1.1x10^{-3}$	1.186×10^{-3}	11.66	0.318	4.42
	Boronized	150.792	445.425	$1.1x10^5$	$4.5x10^{-4}$	3.11×10^{-4}	7.6	0.318	4.5

8.1.2.2 Optical Microscopy.

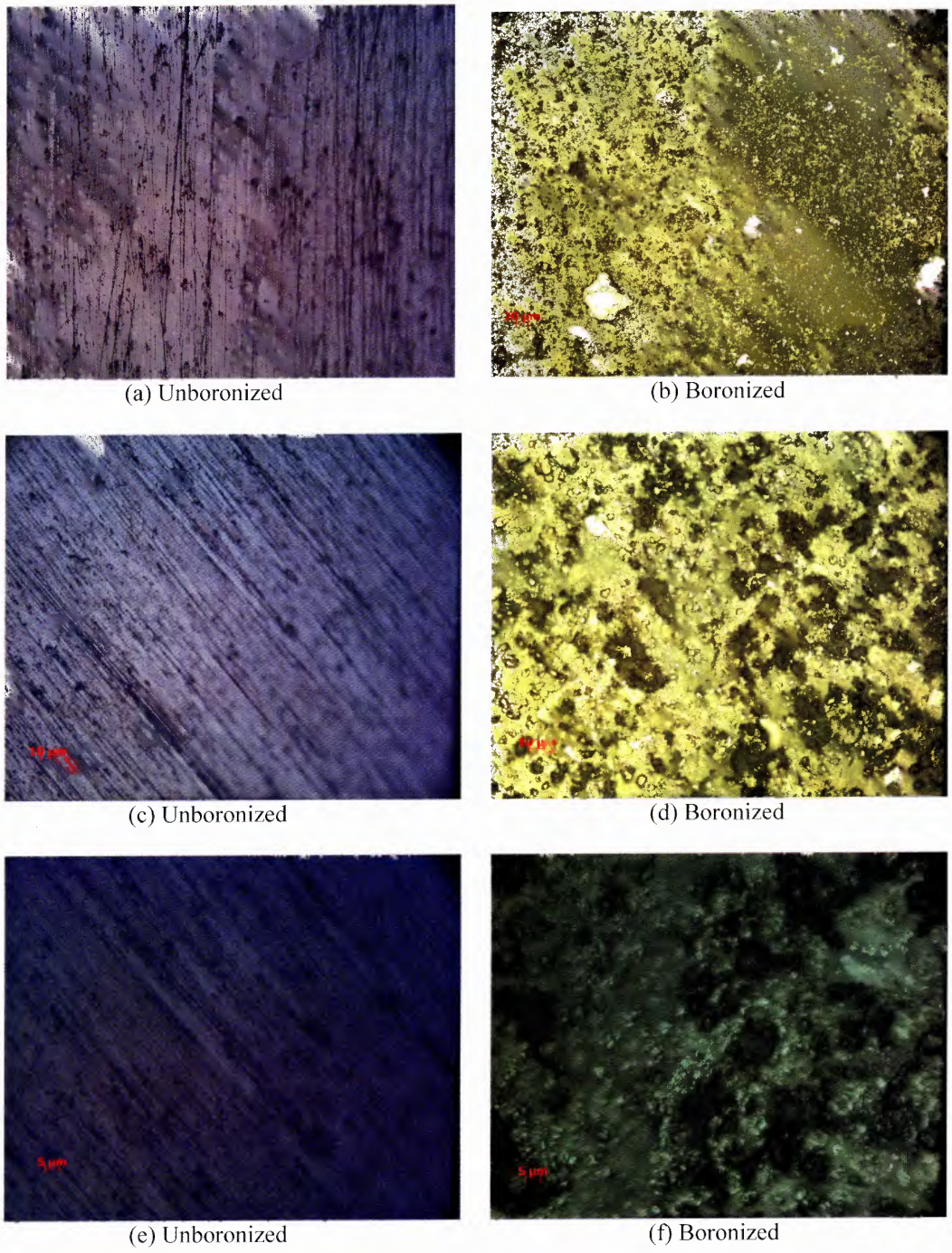

(a) Unboronized (b) Boronized

(c) Unboronized (d) Boronized

(e) Unboronized (f) Boronized

Figure 8.7 Images of titanium alloy samples surfaces at Day 1 prior to corrosion testing in Hank's solution, images (a) and (b) taken at 100x magnification, images (c) and (d) taken at 250x magnification, and images (e) and (f) taken at 500x magnification.

The surface of the unboronized titanium remained unchanged over the 24 hour incubation in Hank's solution, Figure 8.7 (a). The polishing grains were visible and the outlines of grains could be seen, Figure 8.7 (e). The boronized titanium also showed no evidence of change, no change in color or surface defects. The unboronized portion of the boronized sample remained unchanged, the luster of each area remained and signs of corrosion were not present.

8.1.3 Boronized Titanium Alloy Day 4

After the titanium alloy samples were tested at Day 1, they were placed back into the Hank's solution and heated to 37°C for three more days. Corrosion testing and optical images were taken on the fourth day from baseline.

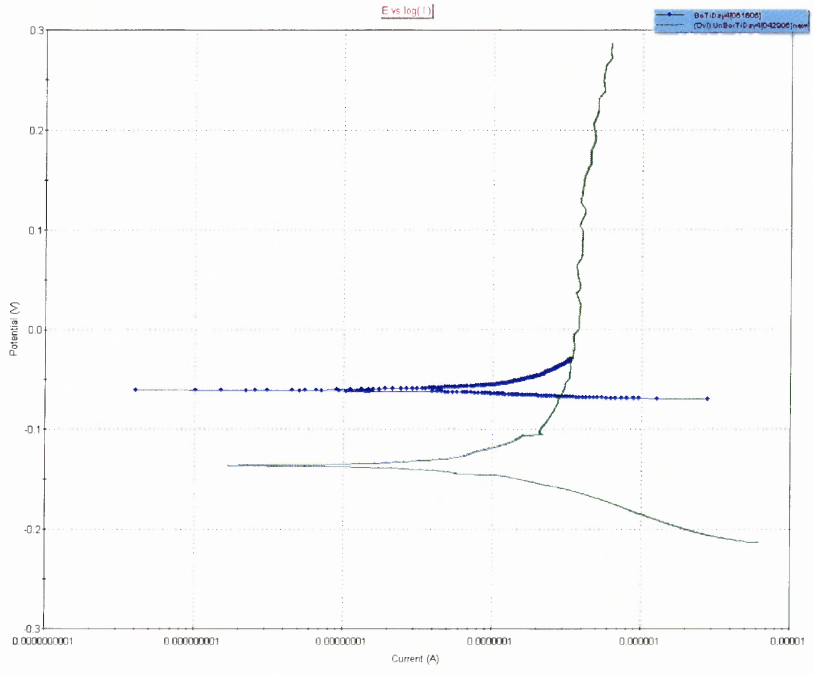

Figure 8.8 Tafel plot at Day 4 for unboronized titanium alloy versus boronized titanium alloy. Boronized titanium alloy is shown in blue, while unboronized titanium alloy is shown in green.

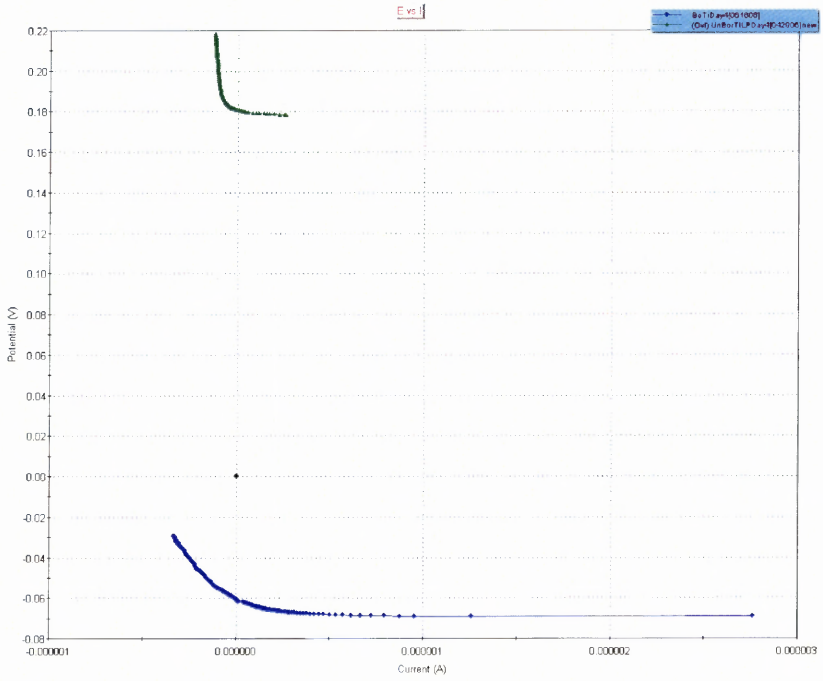

Figure 8.9 Linear polarization plot at Day 4 for unboronized titanium alloy versus boronized titanium alloy. Boronized titanium alloy is shown in blue, while unboronized titanium alloy is shown in green.

The Tafel plot for unboronized titanium alloy shows a non-linear anodic branch. The fluctuations in the anodic branch are a result of the formation and destruction of a passive layer on the surface of the titanium alloy, this occurred as a rest of the sweeping frequency. The potentiostat used a wide range of frequencies and at certain frequencies the passive layer would be created, but at another frequency the passive layer may be destroyed. In Figure 8.8, the unboronized titanium alloy had a lower corrosion potential for the boronized titanium alloy –0.06V compared to the –0.14V of the unboronized titanium alloy. Both the boronized alloy and unboronized titanium alloy showed the same corrosion current (i_{corr}) in the Tafel plot, Figure 8.8, the last time both samples showed the same corrosion current was during baseline testing on Day 0. The change in corrosion potential between Day 4 and Day 1 for the unboronized titanium alloy was a result of damage to the passive oxide layer on the surface of the unboronized titanium. When the

passive layer was damaged, fresh unboronized titanium alloy was susceptible to corrosion, causing a more negative corrosion potential seen in the Tafel plot, Figure 8.8. The boronized titanium alloy graph is depressed because the scale of the unboronized titanium alloy was much larger than the boronized titanium alloy.

The resistance polarization for unboronized titanium alloy was still larger than boronized titanium alloy because a residue of a passive layer was still present on the surface of the unboronized titanium alloy. Titanium oxide is more resistant than titanium boride, because boron is a conductive material.

8.1.3.1 Calculations.

Table 8.6 Experimental and Calculated Corrosion Data at Day 4

Day	Sample	β_X	β_A	Rp (Ω)	Icorr (μA)	Corrosion Rate (MPY)	Equivalent Weight (g)	Area (cm^2)	Density (g/cm^3)
0	Unboronized	113.72	305.797	$2.5x10^5$	$1.5x10^{-4}$	1.62×10^{-4}	11.66	0.318	4.42
	Boronized	182.805	310.422	$2.3x10^5$	$2.2x10^{-4}$	1.5×10^{-4}	7.6	0.318	4.5
1	Unboronized	60.992	642.649	$2.2x10^4$	$1.1x10^{-3}$	1.186×10^{-3}	11.66	0.318	4.42
	Boronized	150.792	445.425	$1.1x10^5$	$4.5x10^{-4}$	3.11×10^{-4}	7.6	0.318	4.5
4	Unboronized	69.097	1276.93	$8.0x10^5$	$3.56x10^{-5}$	$3.84x10^{-5}$	11.66	0.318	4.42
	Boronized	6.499	63.783	$9.6x10^4$	$2.7x10^{-5}$	$1.84x10^{-5}$	7.6	0.318	4.5

8.1.3.2 Optical Microscopy.

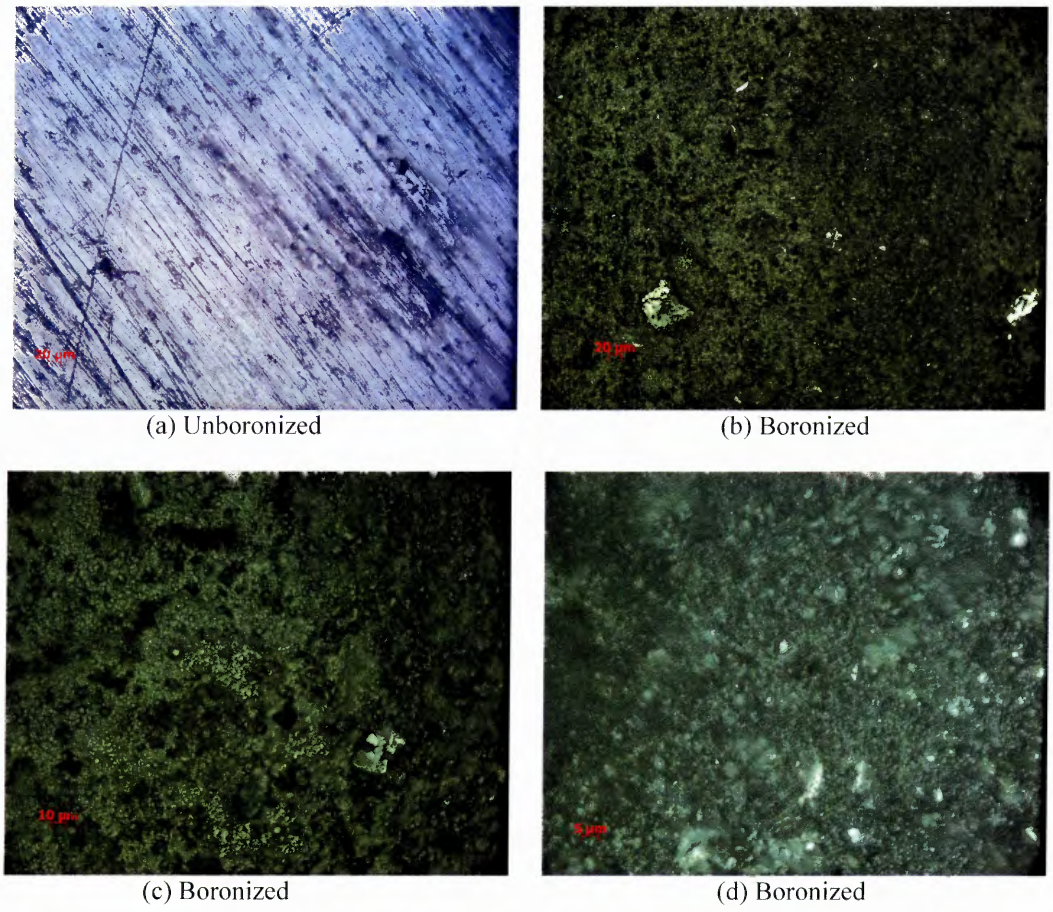

Figure 8.10 Images of titanium alloy sample surfaces at Day 4 prior to corrosion testing in Hank's solution, images (a) and (b) taken at 100x magnification, image (c) taken at 250x magnification, and image (d) taken at 500x magnification.

After four days of incubation in Hank's solution the unboronized titanium alloy, Figure 8.10 (a), shows a diagonal scratch running almost perpendicular to the polishing grain, the diagonal scratch showed a soft passive layer existed on the surface of the unboronized titanium alloy. The grain pattern on the surface was beginning to deepen and show deeper color discoloration. The unboronized titanium alloy in the boronized titanium alloy sample, Figure 8.10 (c) also showed signs of discoloration; the unboronized titanium alloy began to darken and no longer had a luster. The boride layer

was also darker in color. These observations showed that the unboronized titanium alloy was in fact beginning to corrode do to the corrosive environment.

8.1.4 Boronized Titanium Alloy Day 7

Samples tested seven days from baseline time point.

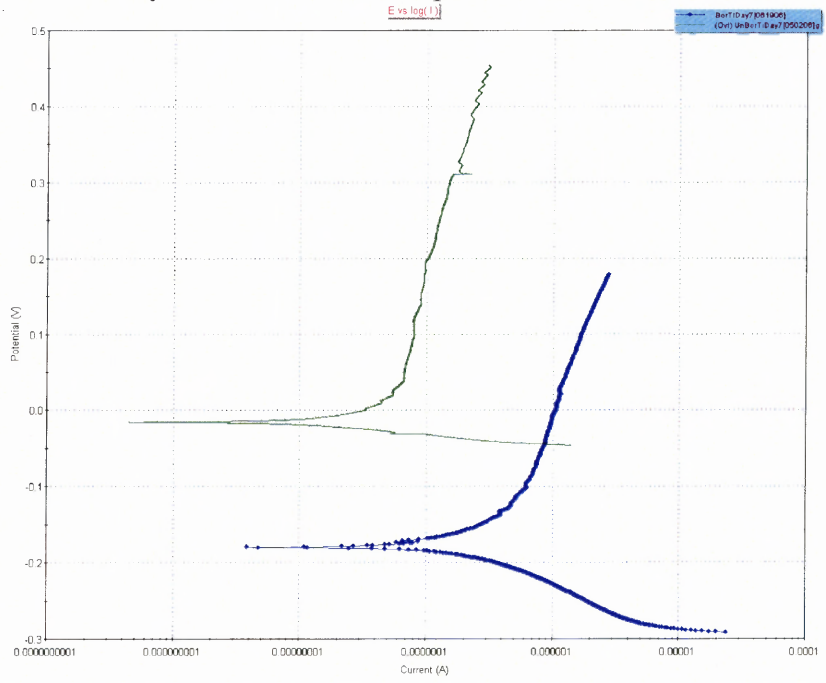

Figure 8.11 Tafel plot at Day 7 for unboronized titanium alloy versus boronized titanium alloy. Boronized titanium alloy is shown in blue, while unboronized titanium alloy is shown in green.

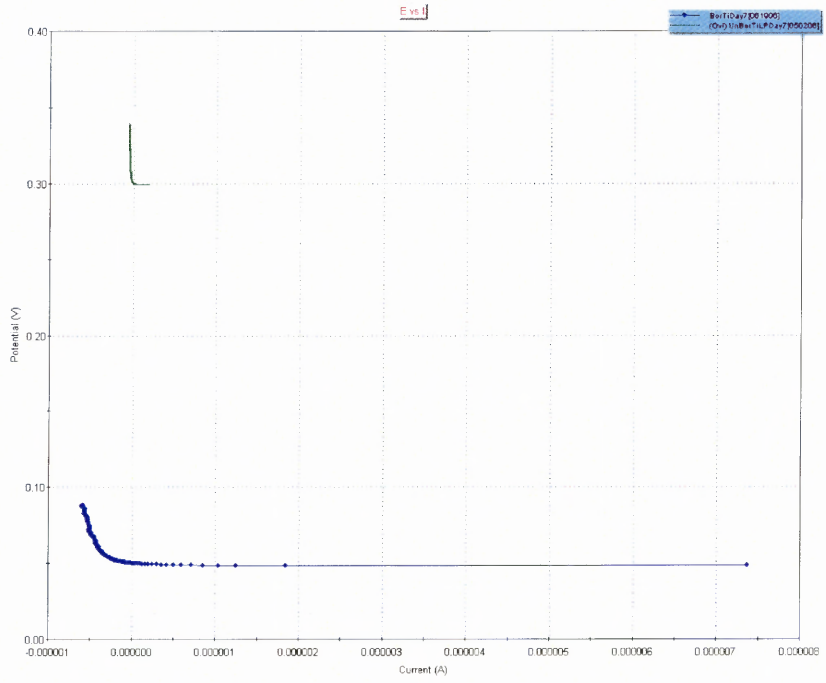

Figure 8.12 Linear polarization plot at Day 7 for unboronized titanium alloy versus boronized titanium alloy. Boronized titanium alloy is shown in blue, while unboronized titanium alloy is shown in green.

8.1.4.1 Calculations.

Table 8.7 Experimental and Calculated Corrosion Data at Day 7

Day	Sample	β_X	β_A	Rp (Ω)	Icorr (μA)	Corrosion Rate (MPY)	Equivalent Weight (g)	Area (cm^2)	Density (g/cm^3)
0	Unboronized	113.72	305.797	$2.5x10^5$	$1.5x10^{-4}$	1.62×10^{-4}	11.66	0.318	4.42
	Boronized	182.805	310.422	$2.3x10^5$	$2.2x10^{-4}$	1.5×10^{-4}	7.6	0.318	4.5
1	Unboronized	60.992	642.649	$2.2x10^4$	$1.1x10^{-3}$	1.186×10^{-3}	11.66	0.318	4.42
	Boronized	150.792	445.425	$1.1x10^5$	$4.5x10^{-4}$	3.11×10^{-4}	7.6	0.318	4.5
4	Unboronized	69.097	1276.93	$8.0x10^5$	$3.56x10^{-5}$	$3.84x10^{-5}$	11.66	0.318	4.42
	Boronized	6.499	63.783	$9.6x10^4$	$2.7x10^{-5}$	$1.84x10^{-5}$	7.6	0.318	4.5
7	Unboronized	27.876	584.03	$1.6x10^6$	$7.07x10^{-6}$	$7.57x10^{-6}$	11.66	0.318	4.42
	Boronized	86.812	416.181	$1.3x10^5$	$2.4x10^{-4}$	$1.7x10^{-4}$	7.6	0.318	4.5

After a week of incubation in Hank's solution, the corrosion rate for boronized titanium was greater than unboronized titanium. The decreased corrosion rate for unboronized titanium was a result of the formation of a passive layer. Over time this passive layer increases in thickness, which caused a decrease in corrosion rate.

8.1.4.2 Optical Microscopy.

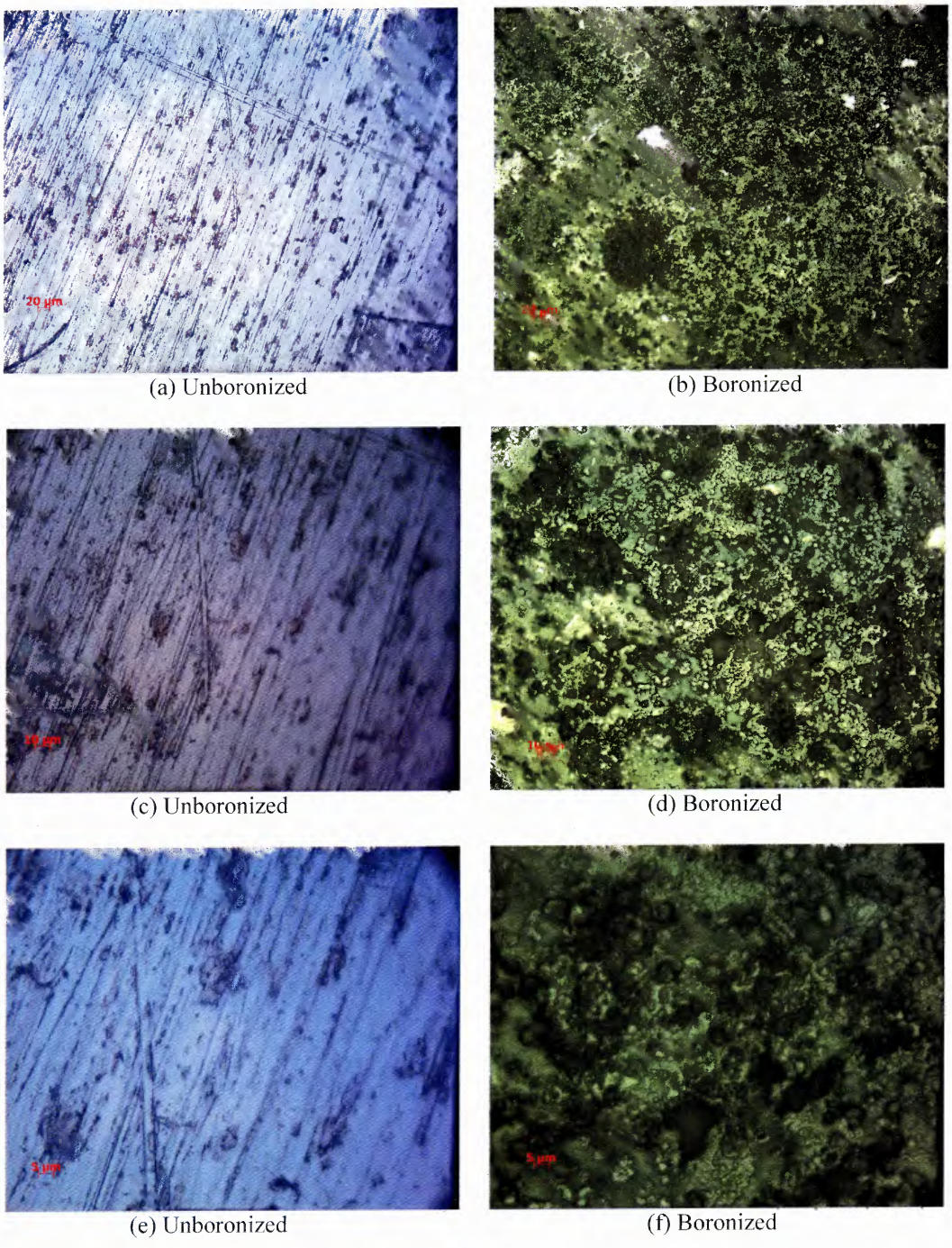

Figure 8.13 Images of titanium alloy samples surfaces at Day 7 prior to corrosion testing in Hank's solution, images (a) and (b) taken at 100x magnification, images (c) and (d) taken at 250x magnification, and images (e) and (f) taken at 500x magnification.

After a week of incubation, the unboronized titanium alloy formed deeper grains and more pits (black points) on the surface. The pits on the surface were the beginning of pitting corrosion. The surface of the unboronized titanium alloy was softer because more perpendicular scratches were found and made in the titanium oxide and titanium dioxide passive layer. Figure 8.13(b,f,e) again demonstrates the 3-dimensional formation of a boride layer. The 3-dimensional boride layer is best seen in Figure 8.13(f), the focused portion of the image is the solid boride layer. The blurred portion of the image is the outer porous boride layer.

8.1.5 Boronized Titanium Alloy Day 14

Samples tested fourteen days from baseline time point.

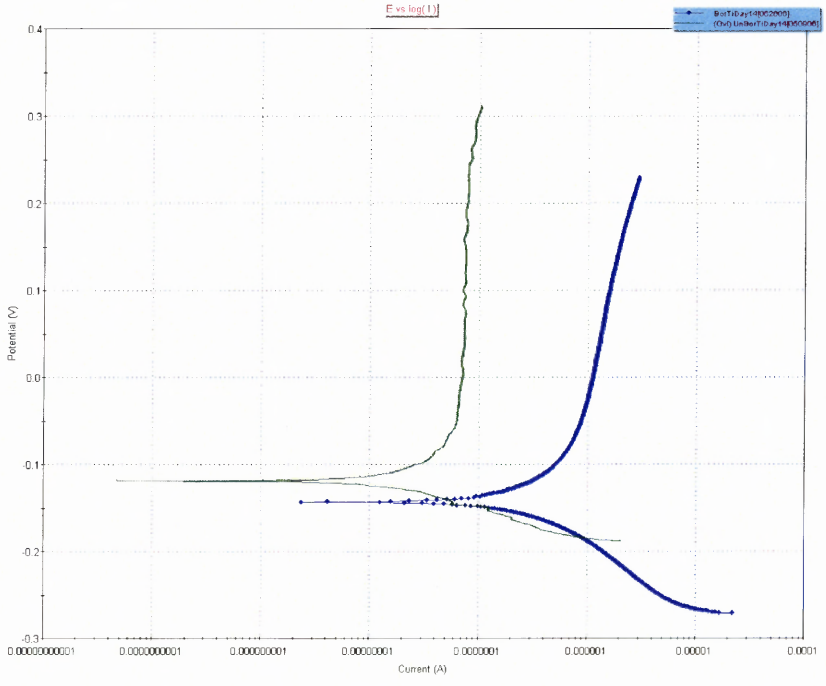

Figure 8.14 Tafel plot at Day 14 for unboronized titanium alloy versus boronized titanium alloy. Boronized titanium alloy is shown in blue, while unboronized titanium alloy is shown in green.

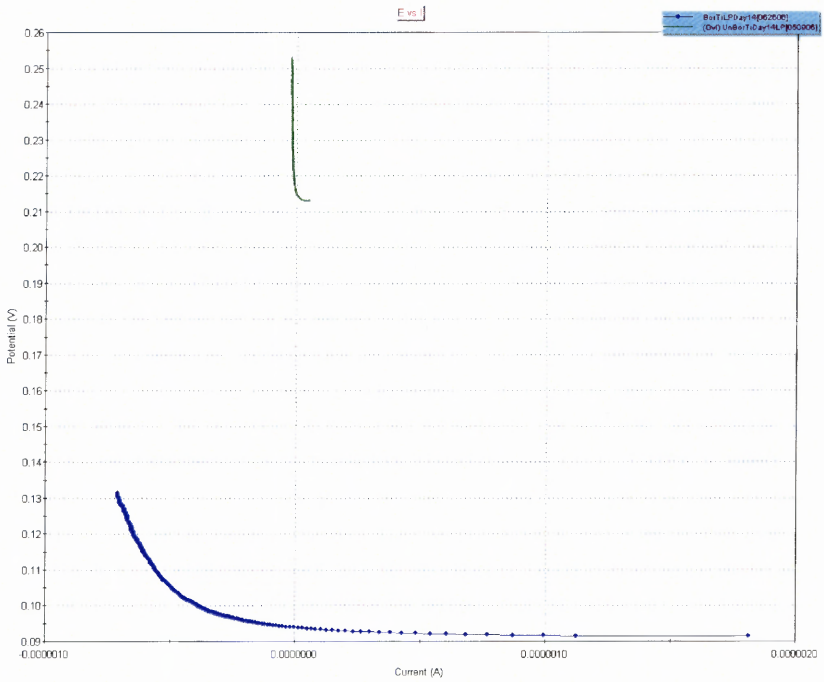

Figure 8.15 Linear polarization plot at Day 14 for unboronized titanium alloy versus boronized titanium alloy. Boronized titanium alloy is shown in blue, while unboronized titanium alloy is shown in green.

The anodic branch of the unboronized titanium alloy in the Tafel plot has a horizontal slope of approximately zero. The cause of the extreme vertical branch is diffusion of solution reactants into the metal substrate. The diffusion of solution reactants into the metal is made possible by the pitting that occurred on the surface of the unboronized titanium alloy. The slope of the anodic branch for boronized titanium alloy does not fluctuate, thus making diffusion for boronized titanium alloy minimal.

8.1.5.1 Calculations.

Table 8.8 Experimental and Calculated Corrosion Data at Day 14

Day	Sample	β_X	β_A	Rp (Ω)	Icorr (μA)	Corrosion Rate (MPY)	Equivalent Weight (g)	Area (cm^2)	Density (g/cm^3)
0	Unboronized	113.72	305.797	$2.5x10^5$	$1.5x10^{-4}$	1.62×10^{-4}	11.66	0.318	4.42
	Boronized	182.805	310.422	$2.3x10^5$	$2.2x10^{-4}$	1.5×10^{-4}	7.6	0.318	4.5
1	Unboronized	60.992	642.649	$2.2x10^4$	$1.1x10^{-3}$	1.186×10^{-3}	11.66	0.318	4.42
	Boronized	150.792	445.425	$1.1x10^5$	$4.5x10^{-4}$	3.11×10^{-4}	7.6	0.318	4.5
4	Unboronized	69.097	1276.93	$8.0x10^5$	$3.56x10^{-5}$	$3.84x10^{-5}$	11.66	0.318	4.42
	Boronized	6.499	63.783	$9.6x10^4$	$2.7x10^{-5}$	$1.84x10^{-5}$	7.6	0.318	4.5
7	Unboronized	27.876	584.03	$1.6x10^6$	$7.07x10^{-6}$	$7.57x10^{-6}$	11.66	0.318	4.42
	Boronized	86.812	416.181	$1.3x10^5$	$2.4x10^{-4}$	$1.7x10^{-4}$	7.6	0.318	4.5
14	Unboronized	28.717	-45000	$5.3x10^5$	$2.35x10^{-5}$	$2.54x10^{-5}$	11.66	0.318	4.42
	Boronized	120.449	$6.20x10^2$	$1.2x10^5$	$3.7x10^{-4}$	$2.6x10^{-4}$	7.6	0.318	4.5

8.1.5.2 Optical Microscopy.

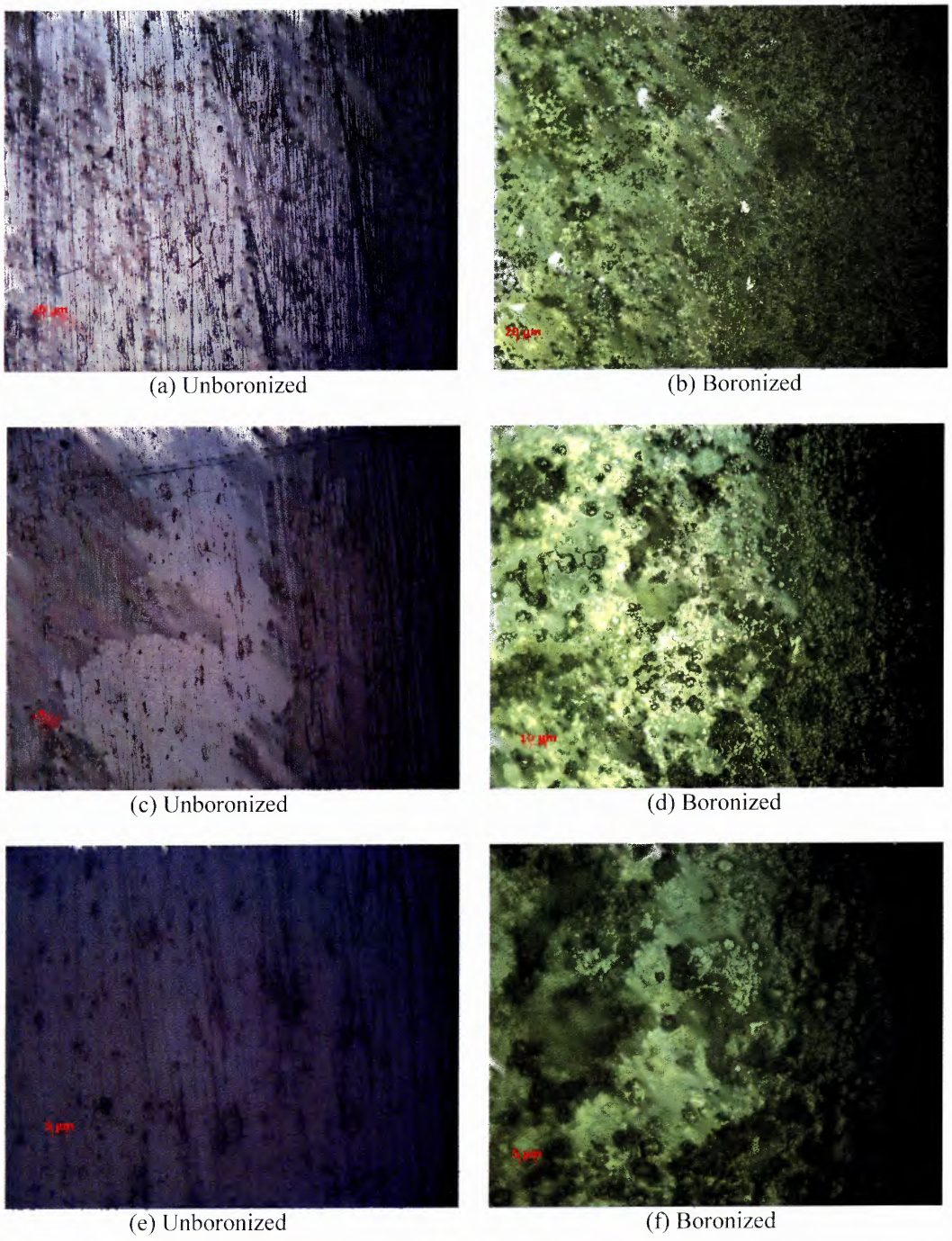

(a) Unboronized (b) Boronized

(c) Unboronized (d) Boronized

(e) Unboronized (f) Boronized

Figure 8.16 Images of titanium alloy samples surfaces at Day 14 prior to corrosion testing in Hank's solution, images (a) and (b) taken at 100x magnification, images (c) and (d) taken at 250x magnification, and images (e) and (f) taken at 500x magnification.

After 14 days of incubation, the surface of the unboronized titanium alloy showed more signs of pitting corrosion as well as deepening of the grains. The pitting and defined grains can further be seen in Figure 8.16(e).

8.1.6 Boronized Titanium Alloy Day 21

Samples tested 21 days from baseline time point.

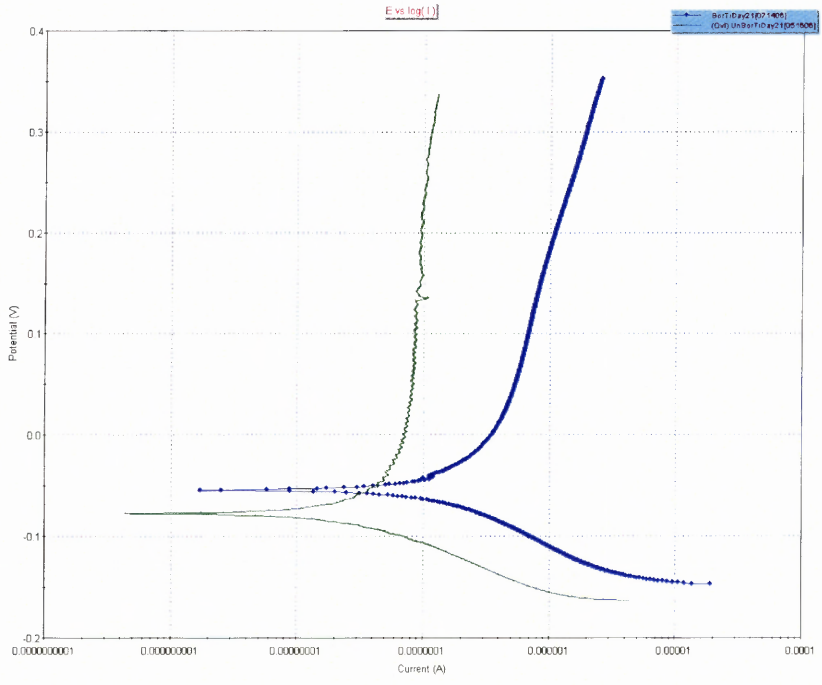

Figure 8.17 Tafel plot at Day 21 for unboronized titanium alloy versus boronized titanium alloy. Boronized titanium alloy is shown in blue, while unboronized titanium alloy is shown in green.

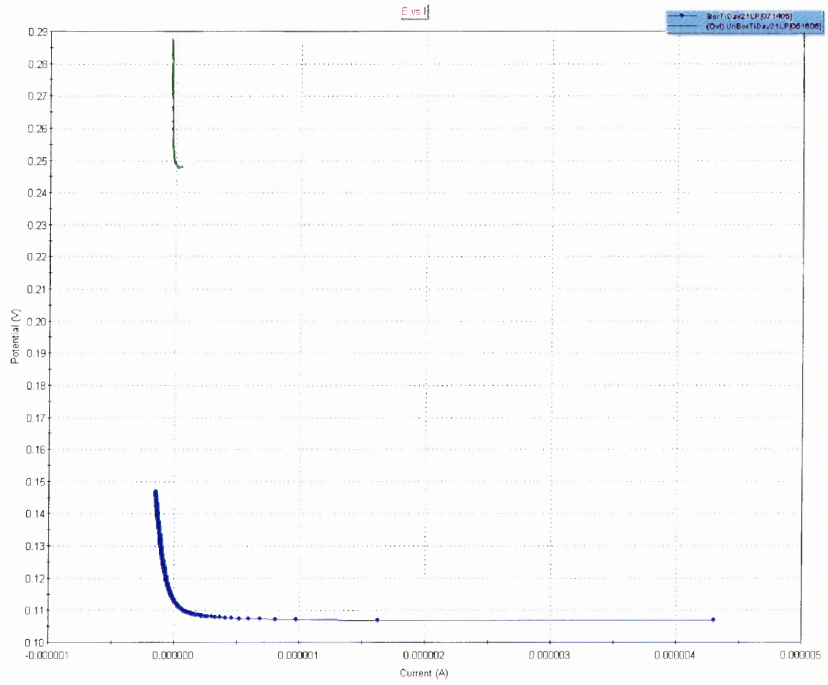

Figure 8.18 Linear polarization plot at Day 21 for unboronized titanium alloy versus boronized titanium alloy. Boronized titanium alloy is shown in blue, while unboronized titanium alloy is shown in green.

After 21 days of incubation, the unboronized titanium alloy had the same zero slope in the anodic branch as Day 14. The continuation of a zero slope anodic branch showed that the diffusion of solution reactants is continuing, thus pitting corrosion was present. The boronized titanium alloy continued to have the same slope as past experiments. The boronized titanium alloy thus showed no sign of layer break down or pitting corrosion.

8.1.6.1 Calculations.

Table 8.9 Experimental and Calculated Corrosion Data at Day 21

Day	Sample	β_X	β_A	Rp (Ω)	Icorr (μA)	Corrosion Rate (MPY)	Equivalent Weight (g)	Area (cm^2)	Density (g/cm^3)
0	Unboronized	113.72	305.797	$2.5x10^5$	$1.5x10^{-4}$	1.62×10^{-4}	11.66	0.318	4.42
	Boronized	182.805	310.422	$2.3x10^5$	$2.2x10^{-4}$	1.5×10^{-4}	7.6	0.318	4.5
1	Unboronized	60.992	642.649	$2.2x10^4$	$1.1x10^{-3}$	1.186×10^{-3}	11.66	0.318	4.42
	Boronized	150.792	445.425	$1.1x10^5$	$4.5x10^{-4}$	3.11×10^{-4}	7.6	0.318	4.5
4	Unboronized	69.097	1276.93	$8.0x10^5$	$3.56x10^{-5}$	$3.84x10^{-5}$	11.66	0.318	4.42
	Boronized	6.499	63.783	$9.6x10^4$	$2.7x10^{-5}$	$1.84x10^{-5}$	7.6	0.318	4.5
7	Unboronized	27.876	584.03	$1.6x10^6$	$7.07x10^{-6}$	$7.57x10^{-6}$	11.66	0.318	4.42
	Boronized	86.812	416.181	$1.3x10^5$	$2.4x10^{-4}$	$1.7x10^{-4}$	7.6	0.318	4.5
14	Unboronized	28.717	-45000	$5.3x10^5$	$2.35x10^{-5}$	$2.54x10^{-5}$	11.66	0.318	4.42
	Boronized	120.449	$6.20x10^2$	$1.2x10^5$	$3.7x10^{-4}$	$2.6x10^{-4}$	7.6	0.318	4.5
21	Unboronized	43.919	1500.72	$5.8x10^6$	$3.18x10^{-6}$	$3.43x10^{-6}$	11.66	0.318	4.42
	Boronized	84.216	440.749	$2.4x10^5$	$1.3x10^{-4}$	$8.67x10^{-5}$	7.6	0.318	4.5

8.1.6.2 Optical Microscopy.

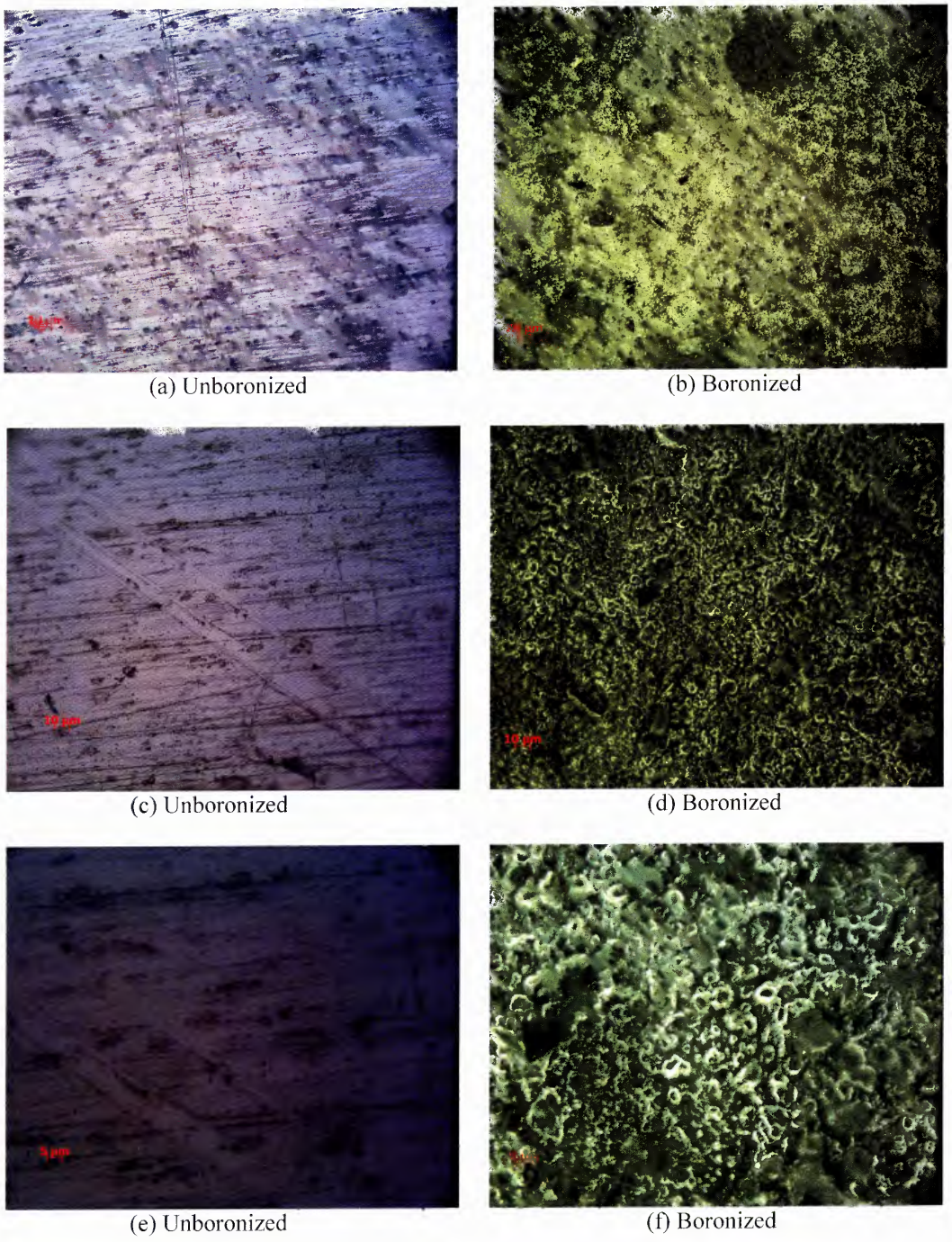

(a) Unboronized (b) Boronized

(c) Unboronized (d) Boronized

(e) Unboronized (f) Boronized

Figure 8.19 Images of titanium alloy samples surfaces at Day 21 prior to corrosion testing in Hank's solution, images (a) and (b) taken at 100x magnification, images (c) and (d) taken at 250x magnification, and images (e) and (f) taken at 500x magnification.

8.1.6.3 Scanning Electron Microscopy. Scanning electron microscopy of both boronized and unboronized titanium alloy was taken to determine whether pitting corrosion occurred on the surface of the titanium as a result of incubating the sample in Hank's solution at 37°C after 21 days. The presence of pitting corrosion is an important characteristic because pitting corrosion can cause the mechanical properties of the metal to decrease, increasing the chances of failure. Pitting corrosion can be determined by many different means, such as cyclic polarization techniques, scanning electron microscopy, and EIS. The downside to using any electrochemical technique is each method requires a new polished unboronized sample as well as a new boronized sample. By using scanning electron microscopy, pitting corrosion can be seen in unboronized and boronized samples used for corrosion testing.

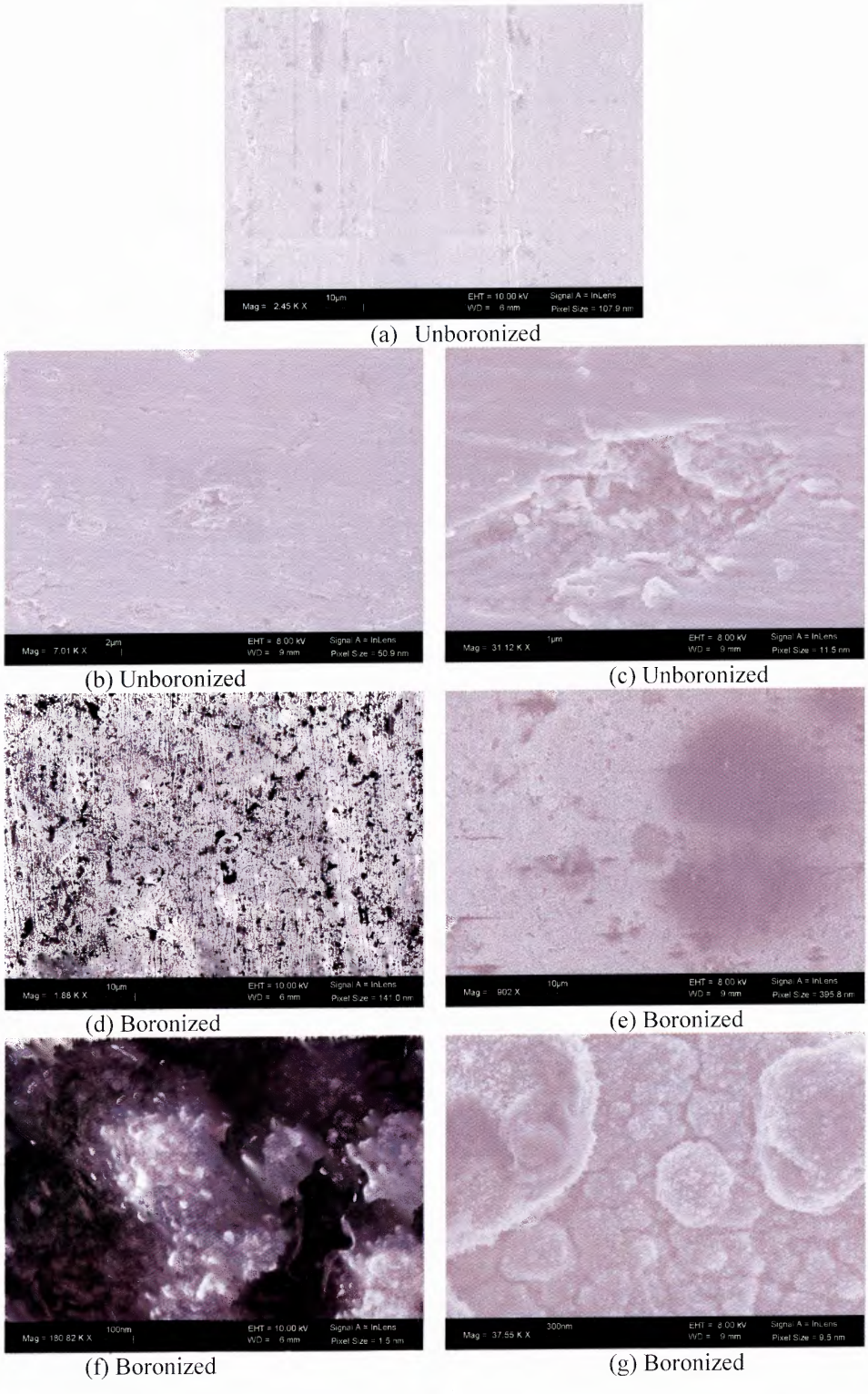

Figure 8.20 Scanning electron microscopy images of unboronized and boronized samples, (a) unboronized sample at Day 0, (b) pitting of unboronized titanium at Day 21, (c) close-up view of pit in surface of unboronized titanium at Day 21, (d) boronized titanium at Day 0, (e) surface of boronized titanium at Day 21, (f) magnified view of titanium boride layer at Day 0, (g) magnified view of titanium boride layer at Day 21.

The scanning electron microscopy images show that over the course of 21 days, the Hank's solution did cause pitting corrosion on the surface of the unboronized titanium alloy, this can be seen in Figure 8.20(b-c). The pitting corrosion demonstrates the passive layer that forms on the surface of the titanium alloy is non-homogeneous and along with pitting corrosion crevice corrosion can occur within this pit. The pitting could also explain the large corrosion resistance fluctuation in unboronized titanium alloy between Day 7 and Day 14.

SEM images of boronized titanium alloy were also taken to look for pitting corrosion and cracking in the boride layer. The SEM images show the boronized titanium alloy does not cover the surface of titanium alloy homogeneously. Figure 8.20(d) shows patches of unboronized titanium alloy because the powder is packed around the polished titanium alloy and the surface is not completely covered with powder. Unlike the unboronized titanium alloy, the boronized titanium alloy does not show signs of pitting corrosion. However, the large dark circular spot in Figure 8.20(e) is a result of the electron beam burning the electrolyte buildup on the surface as a result of incubating in Hank's solution. Finally, the SEM images also show the titanium boride layer forms a three-dimensional structure around the surface of the sample. All of these features are important for analyzing EIS data.

8.2 Summary of Corrosion Degradation Testing

8.2.1 Comparison of Corrosion Rate

Table 8.10 Corrosion Rate Comparison for Entire Degradation Study

Day	Sample	β_C	β_A	Rp (Ω)	Icorr (μA)	Corrosion Rate (MPY)
0	Unboronized	113.72	305.797	$2.5x10^5$	$1.5x10^{-4}$	0.000162
	Boronized	182.805	310.422	$2.3x10^5$	$2.2x10^{-4}$	0.00015
1	Unboronized	60.992	642.649	$2.2x10^4$	$1.1x10^{-3}$	0.001186
	Boronized	150.792	445.425	$1.1x10^5$	$4.5x10^{-4}$	0.000311
4	Unboronized	69.097	1276.93	$8.0x10^5$	$3.56x10^{-5}$	$3.84x10^{-5}$
	Boronized	6.499	63.783	$9.6x10^4$	$2.7x10^{-5}$	$1.84x10^{-5}$
7	Unboronized	27.876	584.03	$1.6x10^6$	$7.07x10^{-6}$	$7.57x10^{-6}$
	Boronized	86.812	416.181	$1.3x10^5$	$2.4x10^{-4}$	$1.7x10^{-4}$
14	Unboronized	28.717	-45000	$5.3x10^5$	$2.35x10^{-5}$	$2.54x10^{-5}$
	Boronized	120.449	6.20x102	$1.2x10^5$	$3.7x10^{-4}$	$2.6x10^{-4}$
21	Unboronized	43.919	1500.72	$5.8x10^6$	$3.18x10^{-6}$	$3.43x10^{-6}$
	Boronized	84.216	440.749	$2.4x10^5$	$1.3x10^{-4}$	$8.67x10^{-5}$

The results of degradation testing showed an interesting trend in the data for unboronized titanium alloy at Day 7 through Day 21. The corrosion current for unboronized titanium shifted from $7.07x10^{-6}$ at Day 7 to $2.35x10^{-5}$ at Day 14 to finally $3.18x10^{-6}$ at Day 21. The cause for the fluctuation in corrosion potential was due to pitting corrosion. Pitting corrosion began on Day 7, the fluctuation in corrosion potential began on Day 7. The increase in corrosion current seen on Day 14 was a result of fresh unboronized titanium being exposed as a result of the pitting corrosion. Finally, the increase of corrosion current on Day 21 was caused by the formation of a passive layer on the walls of the pits formed on Day 7 and 14.

8.2.2 Optical Microscopy

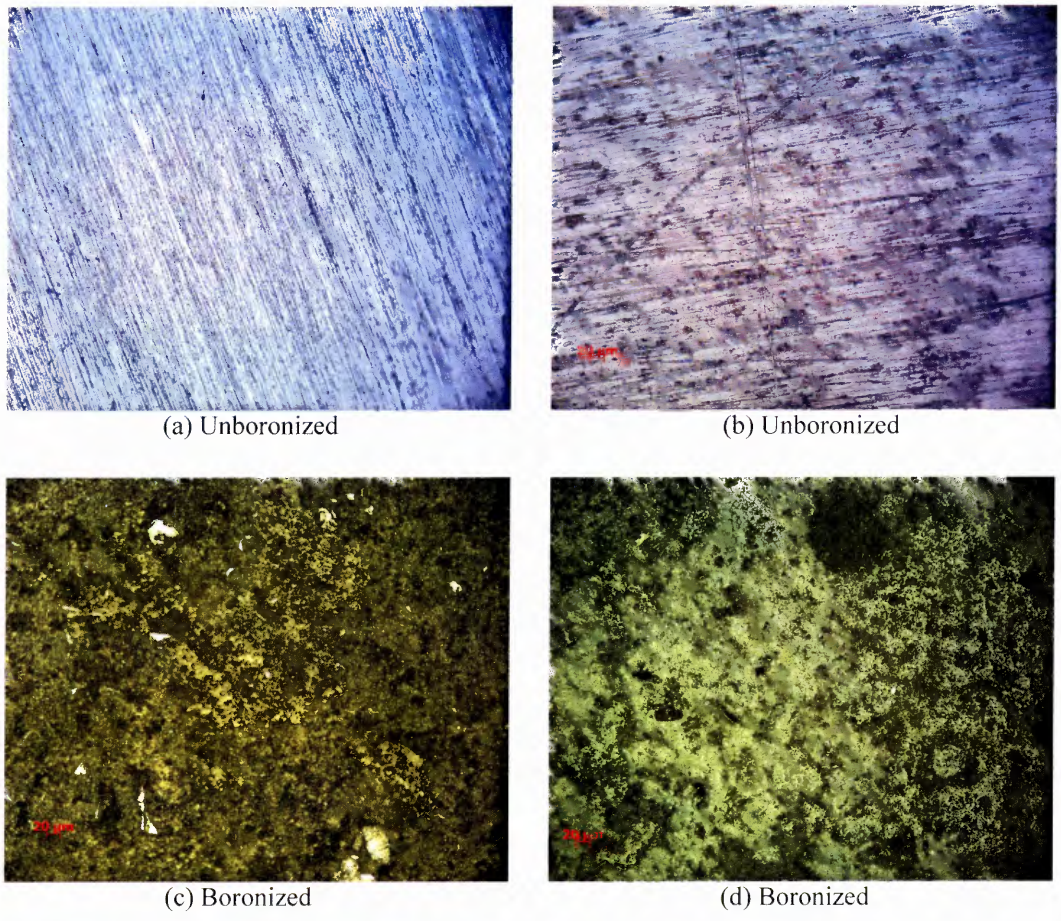

(a) Unboronized (b) Unboronized

(c) Boronized (d) Boronized

Figure 8.21 Optical images of unboronized titanium alloy at Day 0 (a) taken at 100x magnification. Image (b) is the surface of unboronized titanium alloy taken under 100x magnification at Day 21. Image (c) is boronized titanium alloy taken at Day 0 under 100x magnification. Image (d) is boronized titanium alloy taken under 20x magnification at Day 21.

Over the course of 21 days in Hank's solution at 37°C, the unboronized titanium alloy showed signs of pitting corrosion, while boronized titanium alloy remains unchanged. The optical microscopy images taken with 100x magnification in Figure 8.21(a-b) show, how over time, the pitting developed. In Figure 8.21(a) the polished surface of the unboronized titanium alloy has a uniform grain pattern, which is a result of polishing; no perpendicular scratching or pitting was noticed. However, over the course

of the 21-day study, the surface of the unboronized titanium alloy distressed to show black pinhole dots on the surface as well as diagonal and perpendicular scratches.

Unlike the unboronized titanium alloy, the boronized titanium alloy sample showed better weathering over the course of the study. No pitting corrosion was evident on the surface and no boride coating chipped off or scratched. In Figure 8.21(c) areas of unboronized titanium alloy are visible, however, over time the polish titanium alloy is covered. Figure 8.21(d) shows a thicker coating than in Figure 8.21(c) because during degradation calcium, potassium, and magnesium atoms settled onto the boride coating forming a thicker coating. This "salt" coating explains why the surface of the boronized titanium alloy sample burned during SEM imaging after 21 days.

8.3 Passive Layer Formation

Passive layer formation tests the time required for the metal substrate to reach a potential equilibrium. In Figure 8.22 the passive layer formation for both boronized and unboronized titanium alloy are studied. The passive layer formation for unboronized titanium alloy (green line) requires more time than the boronized titanium alloy (blue line), the reason being, the unboronized titanium alloy did not have a protective coating. The boronized titanium alloy already had a protective coating thus explaining the more positive corrosion potential. The passive layer formation on boronized titanium alloy occurred more quickly than unboronized titanium alloy because the boronized titanium alloy graph plateaus sooner than the unboronized titanium alloy. The Open Cell Potential plot concluded that the boronized titanium alloy was more corrosion resistant than the

unboronized titanium alloy because the boronized titanium alloy formed a protective coating sooner than the unboronized titanium alloy.

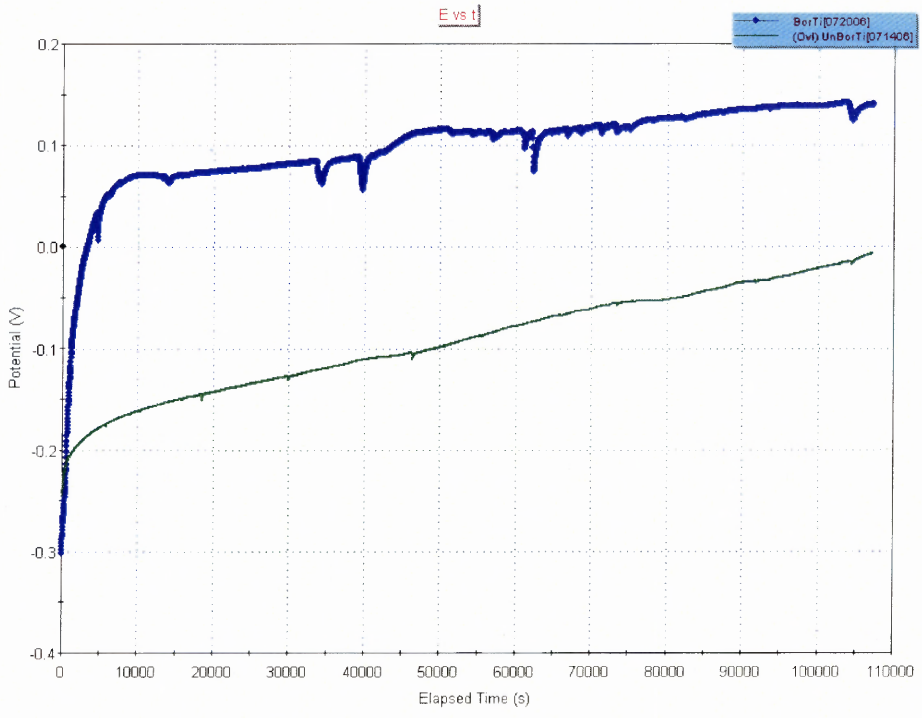

Figure 8.22 Open Cell Potential Plot Used to Measure Passive Layer Formation Time. Boronized titanium alloy is represented by the blue line while unboronized titanium alloy is represented by the green line.

8.4 Electrochemical Impedance Spectroscopy Testing of Boronized Titanium

Electrochemical impedance testing is setup the same way as Tafel and Linear polarization testing. A Princeton Applied Research 2263 series potentiostat and flat cell is used to measure the EIS data. The degradation testing is carried out in the same manner as previously mentioned. Boronized and unboronized samples are placed in Hank's solution for a set period of time at a set temperature of 37°C. Three time periods were measured for EIS: baseline, Day 1 and Day 7.

8.4.1 EIS Data for Boronized Titanium Alloy Day 0

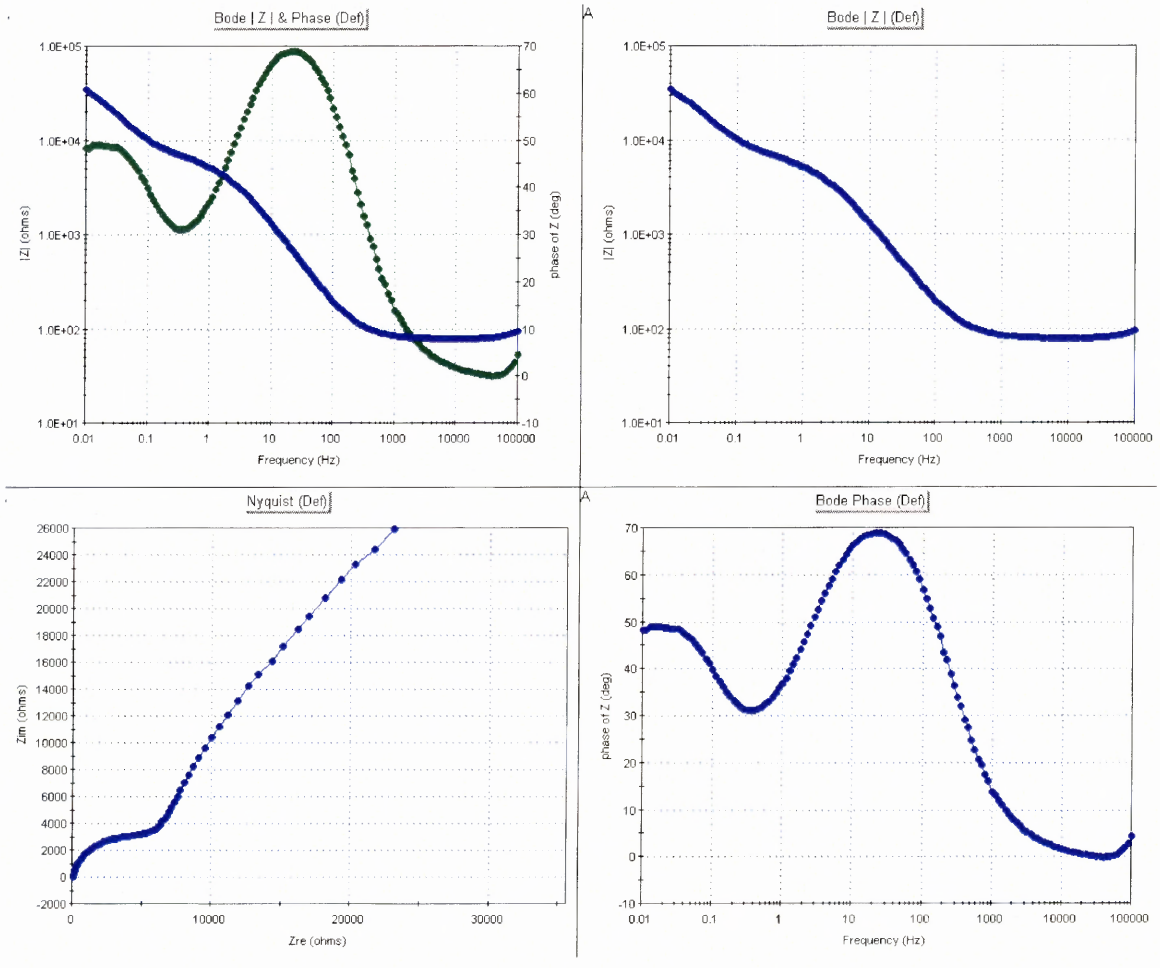

Figure 8.23 Bode and Nyquist plots for boronized titanium alloy Day 0.

Electrochemical impedance spectroscopy testing can explain a lot about a metal's corrosion mechanics. In Figure 8.22, the results of EIS testing (baseline) show the behavior of boronized titanium alloy in a corrosive environment in four separate graphs. The Nyquist plot (lower left graph) shows a semicircle and a 45 degree line; this graph is characteristic of Warburg impedance. Warburg impedance arises when the surface polarization changes as a result of a change in frequency. Warburg impedance mostly occurs in coated metals. The Warburg impedance can also be seen in the Bode Phase graph in the lower right hand corner of Figure 8.22. The y-intercept of the phase plot approaches a phase shift of 45 degrees, this echoes the 45 degree slope seen in the Nyquist graph. Referring to the Bode graph as the frequency increases to higher values the Warburg impedance decreases because the diffusion reactants do not have far to travel to the surface of the metal. However, as the frequency decreases to lower values the Warburg impedance increases. Thus Warburg impedance is inversely proportional to frequency [43]. The amplitude of the peak at lower frequencies signifies the value for the Warburg impedance (W).

The slope of the absolute impedance graph (upper right) shows the existence of a double coating layer, because a small peak exists on diagonal portion of the real Bode plot. The linear portion of the plot signifies a compact passive layer on the surface of the metal. The second peak on the graph at lower frequencies signifies a less compact porous coating layer [33,34]. The boride layer on the surface of the titanium alloy behaves as a capacitor (C_{dl}). The presence of both boride layers is confirmed by optical images taken previously.

The Hank's solution also acts as a resistor (R_Ω) during EIS testing. Because Hank's solution behaves as a resistor, the affects of the electrolytes on the system are seen in the phase graph (lower left). At large frequencies the dip in the phase is caused by the Hank's solution [33,34]. The Nyquist graph finally shows the resistance polarization value (R_p). The resistance polarization is the metals ability to withstand corrosion. Locating the second x-intercept in the Nyquist graph and subtracting off R_Ω can find Rp.

$$R_p = (R_\Omega + R_p) - R_\Omega$$

By analyzing the EIS testing data, a number of equivalent circuit components have been found. By understanding how the overall corrosion system works, equivalent circuit components can be pieced together.

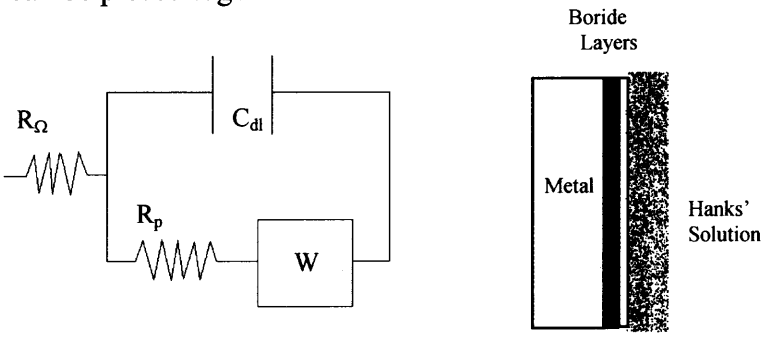

Figure 8.24 Equivalent circuit and system diagram for boronized titanium alloy.

Once a theoretical equivalent circuit was designed the EIS data was analyzed using ZSimpWin (Princeton Applied Research) software. The equivalent circuit was built in the ZSimpWin software and plotted against the measured EIS data. The results of the calculated data versus the measured data are shown in Figure 8.25.

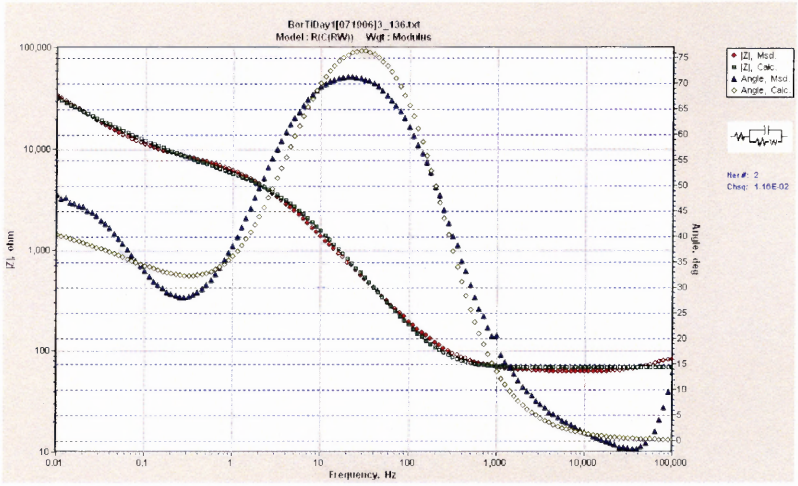

Figure 8.25 Software analysis of EIS data for boronized titanium alloy Day 0.

The green and yellow plot is the calculated portion of the equivalent while the red and blue plots are the measured spectrum of the experiment. The large deviation between the measured and calculated phase shift plots is a result of software limitations due to the version used; a new software version would allow the user to manipulate the EIS data.

Table 8.11 EIS Component Values for Boronized Titanium Alloy Day 0

Measurement	**R_Ω (Ω)**	**C_{dl} (F)**	**R_p (Ω)**	**W ($S*Sec^{1/2}$)**
Measured	78.55	8.274×10^{-6}	7643	0.0001479
Calculated	82.54	9.773×10^{-6}	2914	0.0001302

8.4.2 EIS Data for Unboronized Titanium Alloy Day 0

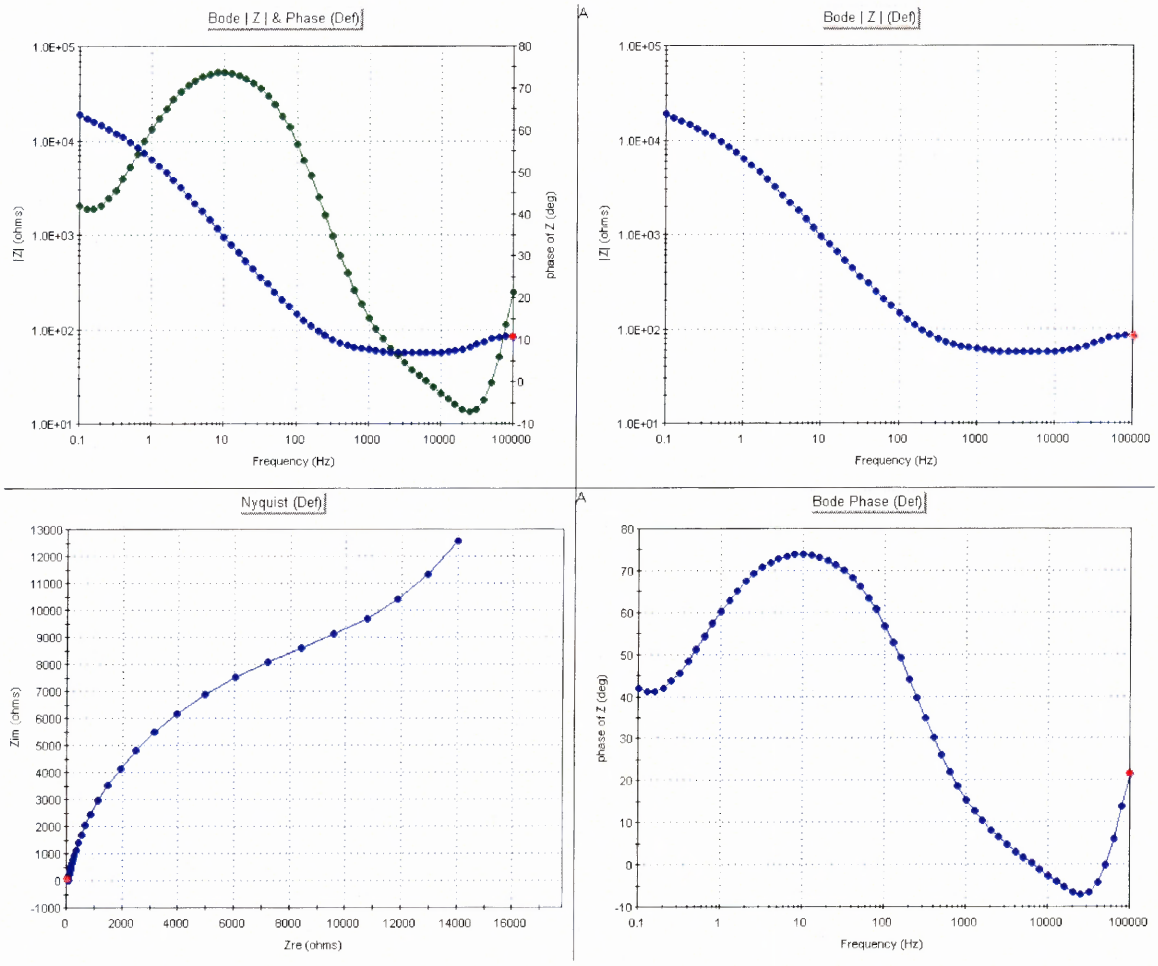

Figure 8.26 Bode and Nyquist plots for unboronized titanium alloy Day 0.

The EIS data for unboronized titanium alloy was analyzed in the same manner as the boronized titanium alloy. The Nyquist plot for unboronized titanium alloy showed a partial semicircle and an increasing slope tail. The diagonal line is not at 45 degrees after a full semi-circle like in the boronized titanium data, thus the unboronized titanium did not show signs of Warburg impedance. The absolute impedance graph (upper right corner) showed a linear slope in the real data plot, which signified a passive layer on the metal has not formed. Since the unboronized titanium alloy was polished before the EIS testing no protective layer was present on the surface, so EIS testing is occurring on the

titanium surface directly. The equivalent circuit that exists for unprotected metals is quite simple; only three components are required. Since unboronized titanium alloy was tested in the same environment as boronized titanium alloy the resistance of Hank's solution must also be taken into consideration. The Hank's solution again behaved as a resistor in the overall corrosion system (R_Ω). The value for R_Ω is calculated by referencing the real component of the Bode plot, the linear portion of the graph at higher frequencies is the value for R_Ω. The metals polarization resistance (R_p) is a property of the titanium alloy and can be calculated by again referring to the absolute impedance component of the Bode plot, the horizontal portion of the real graph at lower frequencies minus the value previously found for R_Ω yields the value for R_p. The capacitance (C_{dl}) is calculated my measuring the slope of the diagonal portion of the real graph in the Bode plot.

Placing the resistors and capacitors of each layer together in parallel, yielded what is known as a Randle Circuit. The Randle Circuit can be seen in Figure 8.27.

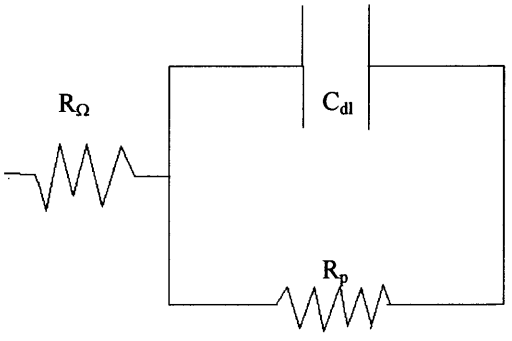

Figure 8.27 Equivalent circuit and corrosion system for unboronized titanium alloy.

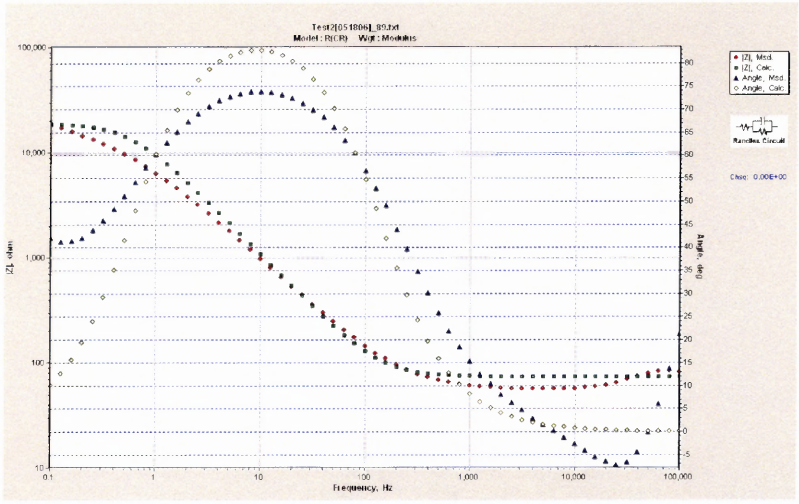

Figure 8.28 Software analysis of EIS data for unboronized titanium alloy Day 0.

Once all of the EIS data were collected the data were exported to ZSimpWin EIS software. The measured data were plotted and the equivalent circuit produced a calculated plot for unboronized titanium alloy. The large dip in the phase shift at large frequencies was a result of the resistance of the Hank's solution. The same dip in phase shift can also be seen in the EIS data for boronized titanium alloy.

Table 8.12 EIS Component Values for Unboronized Titanium Alloy Day 0

Measurement	**R_Ω (Ω)**	**C_{dl} (F)**	**R_p (Ω)**
Measured	74.26	1.5×10^{-5}	18820
Calculated	67.36	1.625×10^{-5}	18430

8.4.3 EIS Data for Boronized Titanium Alloy Day 1

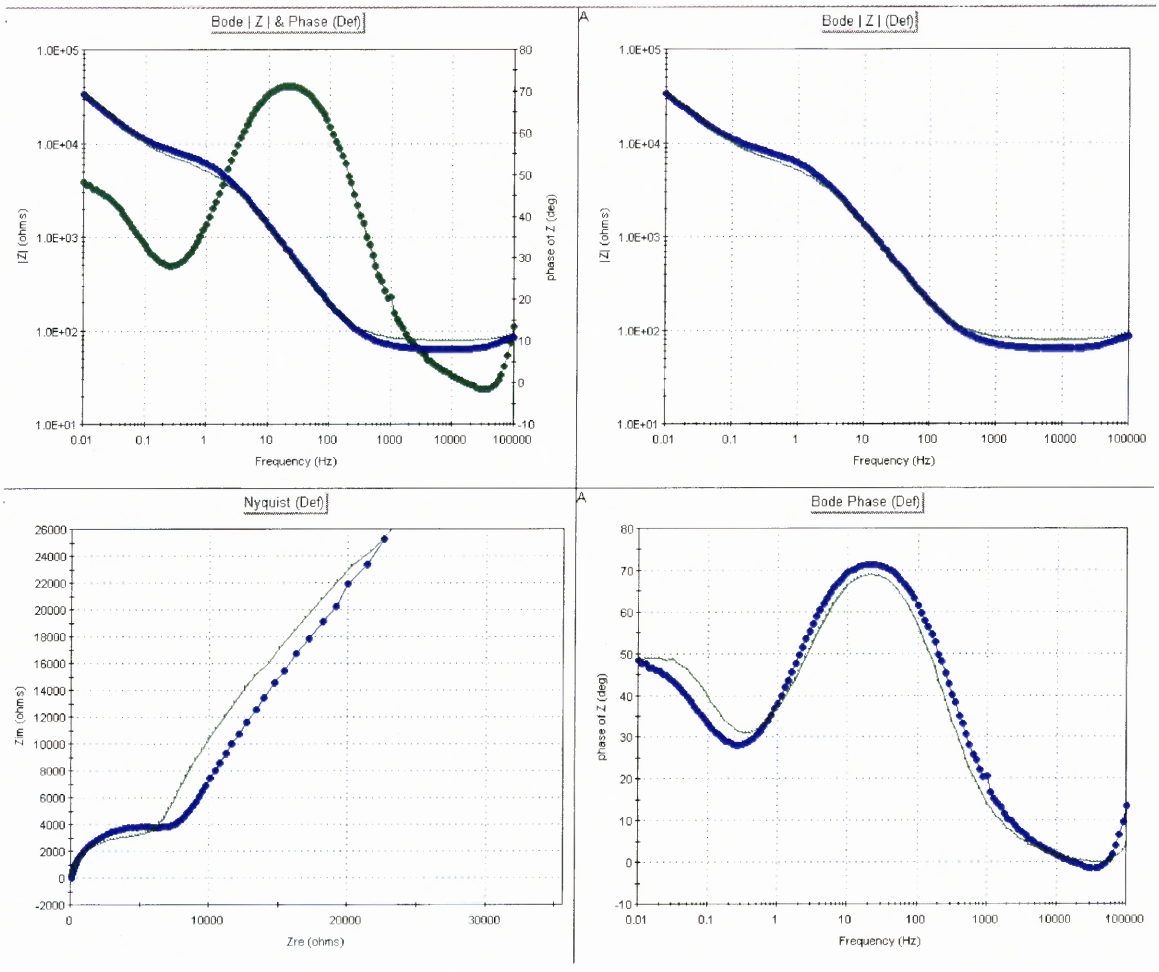

Figure 8.29 Bode and Nyquist plot for boronized titanium alloy at Day 1. Day 1 plot is in bold blue line; the green line represents the data for Day 0.

The EIS data for boronized titanium alloy after 24 hours of incubation showed the same results as the Day 0 testing. The slight drop in Warburg phase shift can be a result of salt residue on the surface of the metal left behind by the Hank's solution. The salt residue may cause the metal surface to be more conductive. The Day 1 data shows the same characteristic dip at high frequencies in the Bode phase shift graph; this same dip can be seen in both unboronized and boronized titanium alloy this reinforces the claim of the Hank's solution as the cause.

Since there was minimal change to the EIS data between Day 0 and Day 1 the equivalent circuit remains the same (Figure 8.24). Only the values for each component of the circuit vary. The calculated EIS plot also matches the measured data much like Day 0.

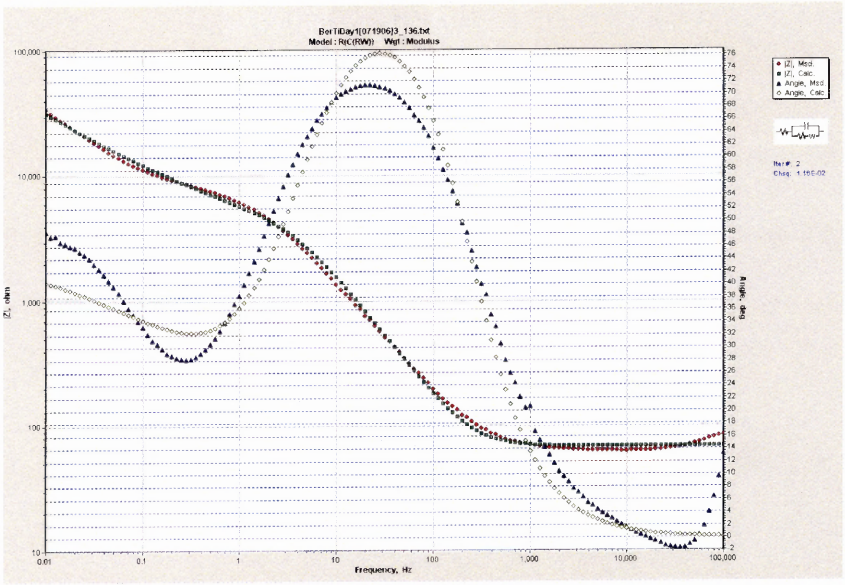

Figure 8.30 Software analysis of EIS data for boronized titanium alloy Day 1.

Due to the minimal changes in component values the calculated EIS data formed by ZSimpWin shows the same outcome as in calculated EIS data for boronized titanium alloy at Day 1. The variation between calculated and measured EIS data is again a result of the software limitations. The software does not allow the user to modify the values for the circuit components directly.

Table 8.13 EIS Component Values for Boronized Titanium Alloy Day 1

Measurement	R_Ω (Ω)	C_{dl} (F)	R_p (Ω)	W (S*Sec$^{1/2}$)
Measured	62.88	1.345 x 10-5	7057	0.0001643
Calculated	69.51	9.523 x 10^{-6}	4310	0.0001363

8.4.4 EIS Data for Unboronized Titanium Alloy Day 1

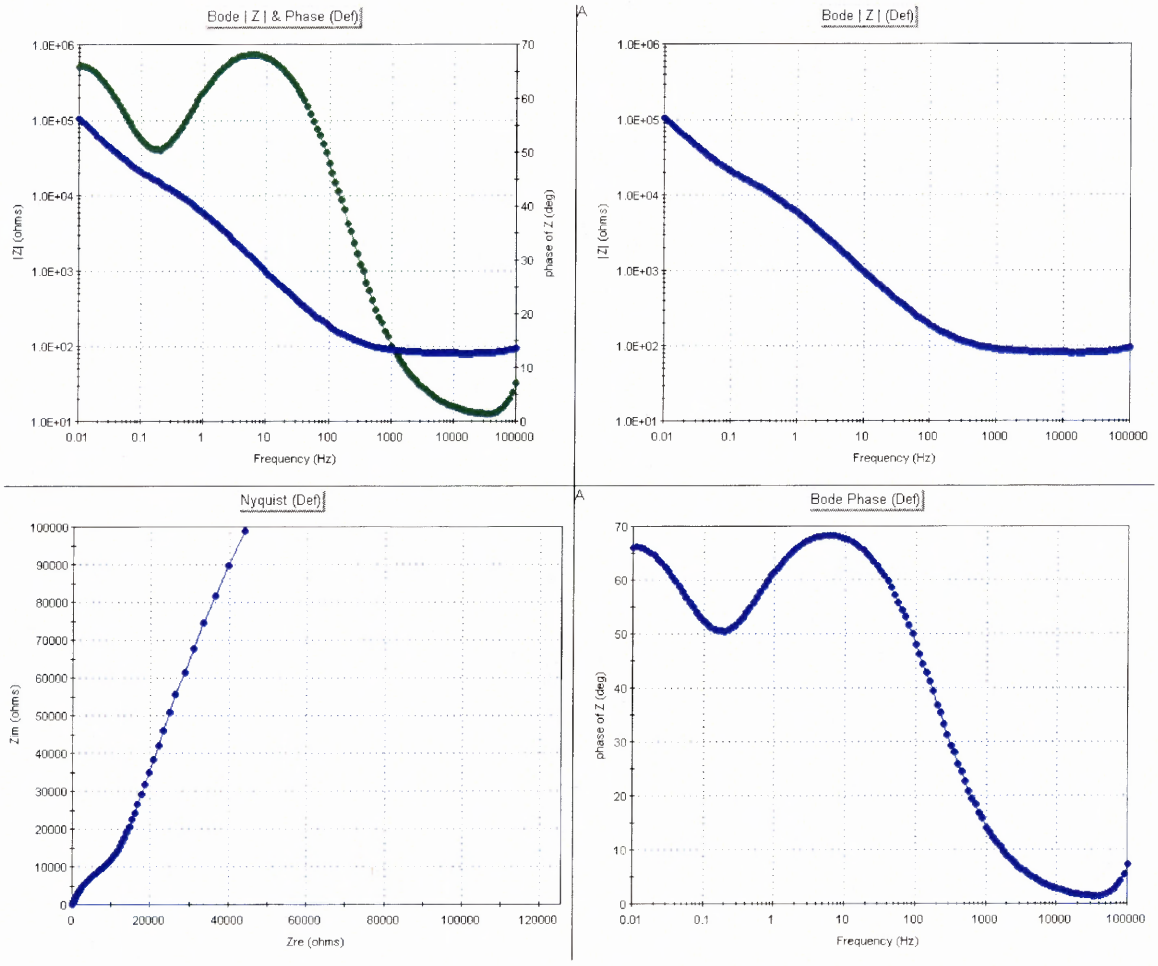

Figure 8.31 Bode and Nyquist plots of unboronized titanium alloy at Day 1.

The EIS data for unboronized titanium alloy at Day 1 can be interpreted a number of ways; the Nyquist plot shows a 45 degree diagonal line which is evidence of a Warburg component. However, the absence of a semi-circle rules out a Warburg component. As degradation time increases the formation of an oxide layer increases, forming a protective layer on the surface of the metal. The absolute impedance portion of the Bode plot shows a small hump at the lower frequencies, this represents the formation of a passive layer, thus adding new components to the equivalent circuit. Both a capacitance (C_{PL}) and a resistance (R_{PL}) is added as a result of the passive layer. The values for polarization

resistance (R_p) and solution resistance (R_Ω) follow the same procedures as in section 8.4.2. The value for passive layer resistance (R_{PL}) is calculated by measuring the magnitude of the near horizontal portion of the absolute impedance plot. The capacitance for both the metal alloy capacitance (C_{dl}) and the passive layer capacitance (C_{PL}) is measured by taking the slope of absolute impedance plot. The larger slope represents the metal alloy capacitance value and the smaller slope represents the value for the passive layer capacitance. The equivalent circuit for unboronized titanium alloy at Day 1 is shown in Figure 8.32.

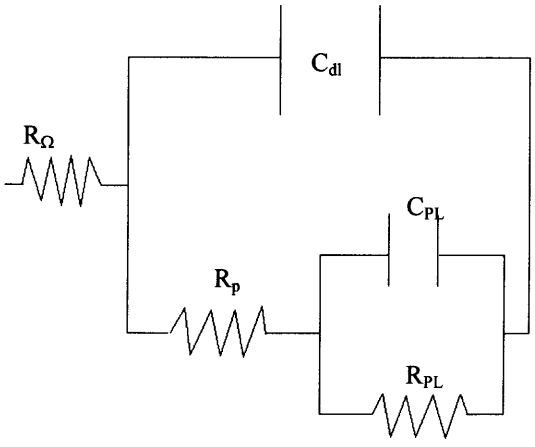

Figure 8.32 Equivalent circuit and corrosion system for unboronized titanium alloy.

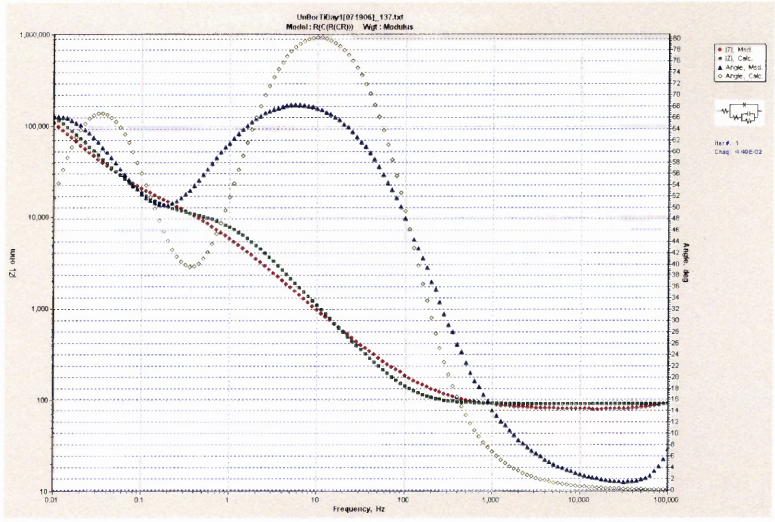

Figure 8.33 Software analysis of EIS data for unboronized titanium alloy Day 1.

Much like the boronized titanium alloy, a protective layer exists on the surface of the metal alloy, consisting of a solid layer containing tiny pores. These tiny pores make the titanium alloy substrate susceptible to pitting corrosion. The electrolyte solution penetrates the pores and concentrates corrosion on a localized area. The solid layer of titanium oxide acts as a capacitor between the surface of the metal alloy (C_{dl}). Since there is a solid layer and pores each behaves as both a resistor and capacitor. Unlike boronized titanium alloy there was no polarization change at the surface of the metal alloy only at each layer of titanium dioxide.

Table 8.14 EIS Component Values for Unboronized Titanium Alloy Day 1

Measurement	R_Ω (Ω)	C_{dl} (F)	R_p (W)	C_{PL} (F)	R_{PL} (Ω)
Measured	81.34	1.72×10^{-5}	13,190	1.152×10^{-8}	18,830
Calculated	92.73	1.475×10^{-5}	12,460	9.625×10^{-5}	20,660

8.4.5 EIS Data for Boronized Titanium Alloy Day 7

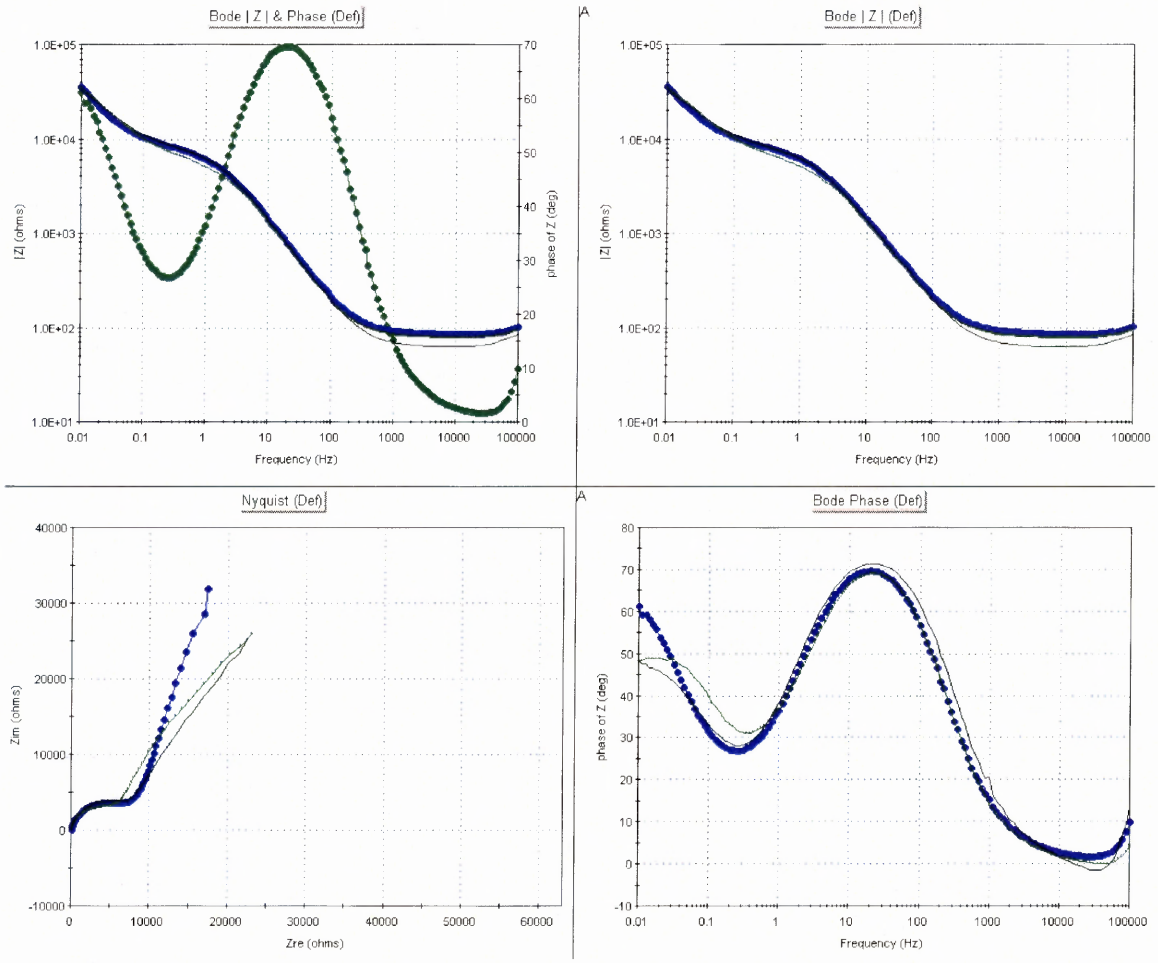

Figure 8.34 Bode and Nyquist plots of boronized titanium alloy at Day 7.

The EIS plot for boronized titanium alloy after 7 days of incubation in Hank's solution shows a modification to the surface coating has occurred. The difference between previous EIS tests for boronized titanium alloy shows a steeper slope in the Nyquist plot. A cause can be residue left behind by the Hank's solution. A new container of Hank's solution was used in this experiment while past testing all used Hank's solution from the same container. A difference between formulation concentrations could cause the steeper slope seen in the Nyquist plot. However, the EIS data for day 7 shows the same behavior as the previous two experiments for boronized

titanium alloy thus the same equivalent circuit components exist; only the values for each component vary.

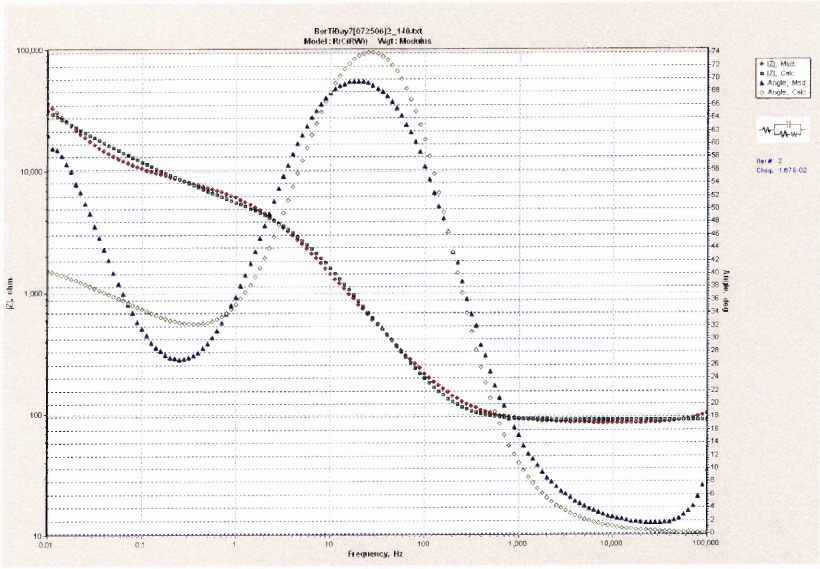

Figure 8.35 Software analysis of EIS data for boronized titanium alloy Day 7.

The imaginary plot of the Bode graph at low frequencies shows an increase from the previous two time points. The phase shift increase is attributed to the deposit of the salt layer on the surface of the boronized titanium alloy. The phase shift increase can also be attributed to the use of a new container of Hank's solution. The resistance of the Hank's solution increased from the previous time points.

Table 8.15 EIS Component Values for Boronized Titanium Alloy Day 7

Measurement	R_Ω (Ω)	C_{dl} (F)	R_p (Ω)	W ($S*Sec^{1/2}$)
Measured	85.27	8.123×10^{-6}	4182	0.0001673
Calculated	100.2	6.647×10^{-6}	2046	0.000085

8.4.6 EIS Data for Unboronized Titanium Day 7

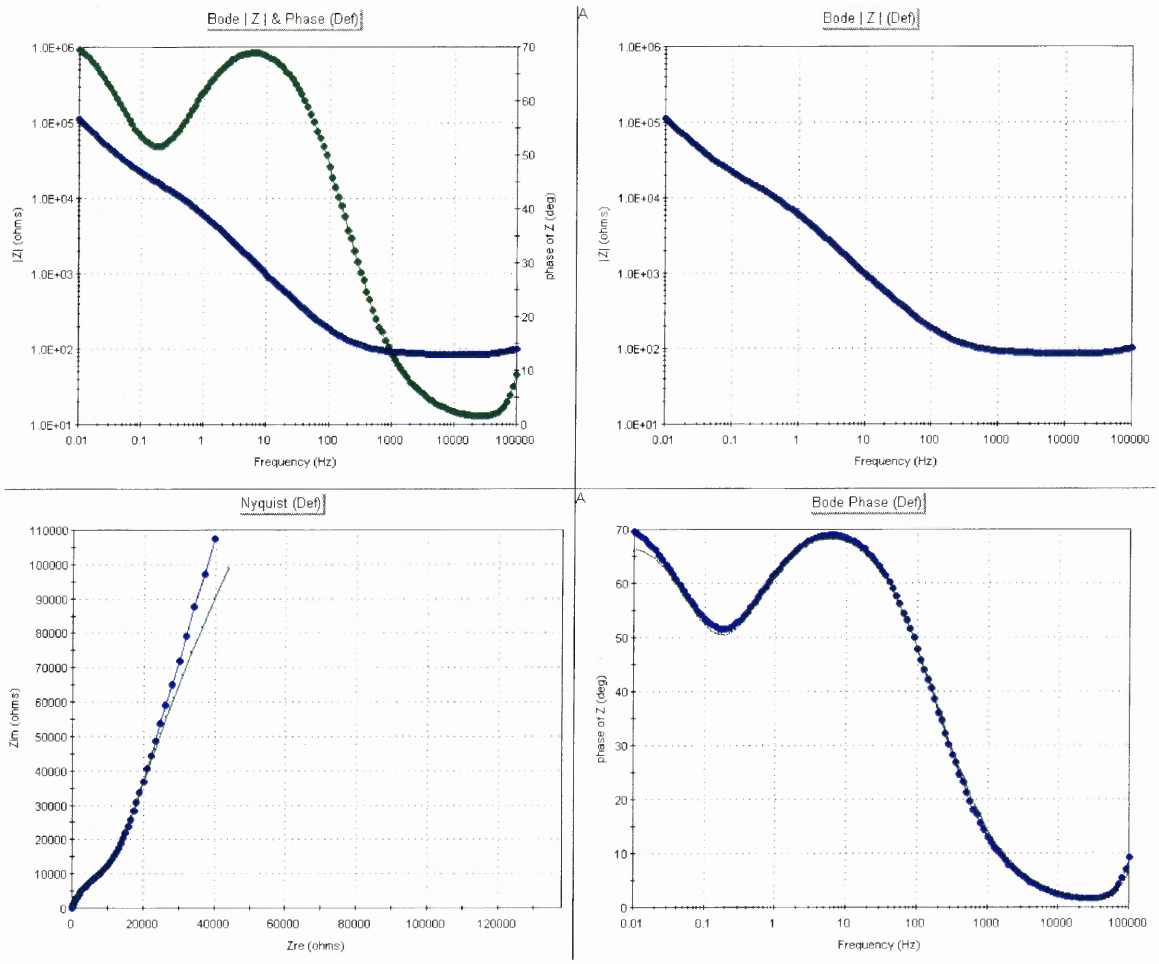

Figure 8.36 Bode and Nyquist plots of unboronized titanium alloy at Day 7.

The EIS data for unboronized titanium alloy after seven days of incubation showed the same behavior as Day 1. The Nyquist plot shows a slight deviation from the data at Day 1, this was a result of thickening of the passive layer on the titanium alloy. The increase in passive layer thickness can be seen when comparing the passive layer resistance (R_{PL}) between Day 1 and Day 7.

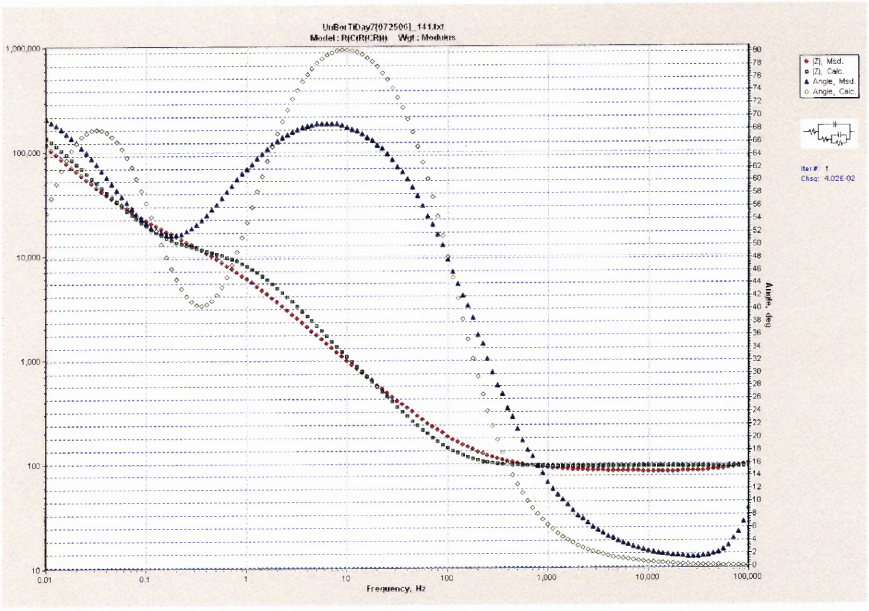

Figure 8.37 Software analysis of EIS data for unboronized titanium alloy Day 7.

The EIS data in ZSimpWin showed a larger variation between calculated and measured data, which was again a result of the increase thickness of a passive layer.

Table 8.16 EIS Component Values

Measurement	R_Ω (Ω)	C_{dl} (F)	R_p (W)	CL (F)	RL (Ω)
Measured	84.99	2.645×10^{-5}	15,310	2.981×10^{-4}	19,145
Calculated	95.43	1.477×10^{-5}	13,220	9.143×10^{-5}	24,460

CHAPTER 9

CONCLUSION

Titanium and titanium alloys are becoming the backbone of medical implants and prosthetics. Titanium and titanium alloys are used because of their high biocompatibility and similarity to bone. However, titanium and titanium alloys also have a low wear resistance. Titanium and titanium alloys are susceptible to particle erosion, which can cause inflammation, infection, and even implant rejection. Boronizing titanium alloy improves titanium's wear resistance and also improves corrosion resistance. Boronized titanium alloy has shown an ability to withstand corrosive environments and pitting corrosion, which is characteristic of standard unboronized titanium alloy. Boronized titanium alloy has proven to be effective in the protection of titanium alloy in-vitro.

Corrosion degradation testing in Hank's solution has only been carried out over the course of 7 days. The degradation testing carried out in this research extended over the course of 3 weeks. By boronizing the surface of the titanium alloy the corrosion rate decreases from 0.00015 MPY at Day 0 to 8.67×10^{-5} MPY at Day 21. The corrosion rate for unboronized titanium alloy decreases from 0.000162 MPY at Day 0 to 3.42×10^{-6} MPY at Day 21. The unboronized titanium alloy showed a smaller corrosion rate at Day 21 than boronized titanium alloy because of a formation of a thick passive layer. The thickness of the passive layer in-vivo would be extremely smaller because the unboronized titanium alloy would be placed under wear rubbing. Thus the corrosion resistance of boronized titanium alloy is higher than in unboronized titanium alloy.

A new technology was used called Electrochemical Impedance Spectroscopy which analyzes the corrosion mechanism of the titanium alloy. This new technology

gives the user an understanding of how the boronized titanium alloy behaves in a corrosive environment. A benefit of this technology is a representation of the corrosion system can be made and studied; this representation is called an equivalent circuit. EIS testing has never been conducted on boronized titanium alloy, thus making this research critical for understanding the effects of a boron coating on titanium alloy.

EIS testing produced an equivalent circuit for boronized titanium alloys showing that a protective layer of boride was present on the surface, and over time this layer protects the titanium alloy in the entirety over the course of the corrosion study. Since, the boride layer remained unchanged the equivalent circuit for boronized titanium alloy remained the same for the entire EIS degradation study. However, the unboronized titanium alloy began to show signs of pitting corrosion and the equivalent circuit for unboronized titanium alloy changed after 24 hours of incubation. This proves that the boron layer on titanium alloy is useful in preventing corrosion of titanium alloys used for biomedical implants.

CHAPTER 10

FUTURE WORK

In-vitro characterization is just the beginning of the characterization needed before a true understanding of boronized titanium alloy as a medical implant can be found. A number of critical characterization studies need to be performed such as:

- Passive film rub testing on both the unboronized titanium alloy and boronized titanium alloy.

  Study aimed to understand the effects of wear on the passive layer on both titanium alloy samples. Could prove boronized titanium alloy to be even more corrosive resistant compared to unboronized titanium alloy. Using a Sutherland Rub Tester, rub testing simulates rubbing of a ball in socket joint found in hip replacement.

- Longer incubation periods on corrosion testing.

  Gives a better understanding of the effects of corrosion on boronized titanium alloy at longer time points. Gives insight to whether pitting corrosion does occur in boronized titanium alloy over time.

- Corrosion testing on hydroxyapatite and collagen coated boronized titanium alloy.

  Gives an understanding of the corrosive properties of hydroxyapatite and collagen. Do the coatings provide extra protection?

- In-vivo testing for understanding of histological and physiological effects.

  Performing in-vivo characterization is the most important study remaining. In-vivo testing will give an understanding of the effects of tissue reaction, toxicity, physiological abnormalities, tissue adhesion, and implant rejection.

REFERENCES

[1] M. J. Donachie, "Titanium," Metals Handbook, Ninth edition, Volume 3, Pages 9.1-9.12.

[2] American Society of Metals International, *ASM-Engineered Materials Reference Book*, 2nd Edition, 1994.

[3] G. S. Brady and H. R. Clauser, *Materials Handbook*, 13th Edition, New York: McGraw-Hill, 1991. Pages 843-846.

[4] W. F. Smith, *Foundations of Materials Science and Engineering,* 3rd Edition, New York: McGraw-Hill, 2004.

[5] W. D. Callister, *Materials Science and Engineering: An Introduction,* 6th Edition, New York: Jon Wiley and Sons, 2003.

[6] R. G. Munro, "Material Properties of Titanium Diboride," *Journal of Research of the National Institute of Standards and Technology.* Volume 105, Number 5, 2000. Pages 709-720.

[7] E. Jelis, N. Suwattananont, and R. Petrova, "Boronizing of Ti-6Al-4V Eli by Powder Pack Method for Biomedical Application," Northeast Biomedical Conference.

[8] S. Pilar, M. Patel, and E. Jelis, "*Design of a New Approach to Boronize Ti-6Al-4V (ELI) for Biomedical Applications.*" Senior Thesis. Newark NJ, New Jersey Institute of Technology Department of Biomedical Engineering.

[9] P. A. Dearnley and T. Bell, "Engineering the Surface with Boron Based Materials," *Surface Engineering*, Volume 1, Number 3, Pages 203-217.

[10] N. Suwattananont, "Surface Treatment of Ferrous Alloys with Boron," Thesis, 2004, Newark, NJ. New Jersey Institute of Technoloy.

[11] R. Chatterjee-Fischer, "Boriding and Diffusion Metallizing," *Surface Modification Technologies*. New York: Marcel Dekker, 1989. Pages 567-609.

[12] A. O. Prytula, I. M. Pohrelyuk, and O. I. Yas'kiv, "Investigation of the Surface Layers of Titanium After Thermodiffusive Saturation in a Boron-Coating Medium," *Materials Science*. Volume 40, Number 1, 2004. Pages 60-64.

[13] E. Rodriguez-Cabeo, G. Laudien, S. Biemer, K.T. Rie, S. Hoppe, "Plasma-assisted boriding of Industrial Components in a Pulsed D.C. glow discharge." *Surface and Coatings Technology.* Volume 116-119, 1999, Pages 229-233.

[14] K. G. Anthymidis, E. Stergioudis, D. N. Tsipas, "Boriding in a Fluidized Bed Reactor," *Materials Letters.* Volume 51, 2001, Pages 156-160.

[15] C. M. Schoenfeld, E. P. Lautenschlager, and P. R. Meyer, " Mechanical Properties of Human Cancellous Bone in the Femoral Head." *Journal of Medical and Biological Engineering*, Volume 12, Number 3, Pages 313-317, May 1974.

[16] S. M. Tommasini, P. Nasser, M. B. Schaffler, and K. J. Jepsen, "Relationship Between Bone Morphology and Bone Quality in Male Tibias: Implications for Stress Fracture Risk." *Journal of Bone and Mineral Research.* Volume 20, Number 8, Pages 1372-1380, March 2005.

[17] H. H. Bayraktar, E. F. Morgan, G. L. Niebur, G. E. Morris, E. K. Wong, T. M. Keaveny, "Comparison of the Elastic and Yield Properties of Human Femoral Trabecular and Cortical Bone Tissue." *Journal of Biomechanics.* Volume 37, Pages 27-35, June 2004.

[18] J. B. Park and R.S. Lakes, *Biomaterials: An Introduction*, 2nd Edition , New York: Plenum Press, 1992.

[19] J. Blitz, K. Goswami, and V. Ammatathonchai, "*The Design and Testing of a New Hydroxyapatite Coating for Pack Boronized Ti-6Al-4V to be used for Medical Implant Materials.*" Senior Thesis, Newark NJ. New Jersey Institute of Technology, Department of Biomedical Engineering.

[20] M. Katto, M. Nakanura, T. Tanaka, T. Nakayama, "Hydroxyapatite Coatings Deposited by Laser-Assisted Laser Ablation Method." *Applied Surface Science.* Volume 197-198, Pages 768-771, 2002.

[21] G. Goller, R. N. Oktar, L. S. Ozyegin, E. S. Kayali, E. Demirkesen, " Plasma-sprayed Human Bone-derived Hydroxyapatite Coatings: Effective and Reliable." *Materials Letters.* Volume 58, Pages 2599-2604, 2004.

[22] J. Dumbleton and M. T. Manley, " Hydroxyapatite-Coated Prostheses in Total Hip and Knee Arthroplasty." *Journal of Bone and Joint Surgery.* Volume 86A, Number 11, Pages 2526-2540, November 2004.

[23] D. A. Jones, *Principles and Prevention of Corrosion*, 2nd Edition, Saddle River, NJ: Prentice Hall, 1996.

[24] R. Vangaveti, "Boron Induced Surface Modification of Transition Metals," M.S. Thesis, 2005, Newark, NJ. New Jersey Institute of Technology.

[25] K. Pallegar, " Electrochemical Corrosion Testing of Boronized and Unboronized Steels," M.S. Thesis 2005, Newark, NJ. New Jersey Institute of Technology.

[26] Princeton Applied Research Application Notes Corr-4, "Electrochemistry and Corrosion Overview and Techniques." http://www.princetonappliedresearch.com/

[27] S. Luiz de Assis, S. Wolynec, and I. Costa, "Corrosion Characterization of Titanium Alloys by Electrochemical Techniques." *Electrochimica Acta.* February 2005.

[28] I. Milosev, M. Metikos-Hukovic, and H. H. Strehblow, " Passive Film on Orthopaedic Ti-Al-V Alloy formed in Physiological Solution Investigated by X-Ray Photoelectron Spectroscopy." *Biomaterials.* Volume 21, Pages 2103-2113, April 2000.

[29] C. X. Wang, M. Wang, and X. Zhou, "Nucleation and Growth of Apatite of Chemically Treated Titanium Alloy: An Electrochemical Impedance Spectroscopy Study." *Biomaterials.* Volume 23, Pages 3069-3077, March 2003.

[30] M. Aziz-Kerrzo, K. G. Conroy, A. M. Fenelon, S. T. Farrell, and C. B. Breslin. "Electrochemical Studies on the Stability and Corrosion Resistance of Titanium-Based Implant Materials." *Biomaterials.* Volume 22, Pages 1531-1539, September 2000.

[31] A. K. Shukla and R. Balasubramaniam, "Effect of Surface Treatment on Electrochemical Behavior of CP Ti, Ti-6Al-4V, and Ti-13Nb-13Zr Alloys in Simulated Human Body Fluid." *Corrosive Science.* June 2005.

[32] F. Contu, B. Elsener, H. Bohni, "Serum Effect on the Electrochemical Behavior of Titanium, Ti-6Al-4V, and Ti-6Al-7Nb Alloys in Sulphuric Acid and Sodium Hydroxide." *Corrosion Science.* Volume 46, Pages 2241-2254, February 2005.

[33] M. V. Popa, I. Demetrescu, E. Vasilescu, P. Drob, A. S. Lopez, J. Mirza-Rosca, C. Vasilescu, and D. Ionita, "Corrosion Susceptibility of Implant Materials Ti-5Al-4V and Ti-6Al-4Fe in Artificial Extra-Cellular Fluids." *Electrochimica Acta.* Volume 49, Pages 2113-2121, December 2003.

[34] I. Gurappa, "Characterization of Different Materials for Corrosion Resistance Under Simulated Body Fluid Conditions." *Material Characterization.* Volume 49, Pages 73-79, September 2002.

[35] A. K. Shukla, R. Balasubramaniam, S. Bhargava, "Effect of Replacement of V by Fe and Nb on Passive Film Behavior of Ti-6Al-4V in Simulated Body Fluid Conditions." *Journal of Alloys and Compounds.* Volume 389, Pages 144-152, August 2004.

[36] Y. Khelfaoui, M. Kerkar, A. Bali, F. Dalard, "Electrochemical Characterisation of a PVD Film of Titanium on AISI 316L Stainless Steel." *Surface & Coatings Technology.* Volume 200, Pages 4523-4529, March 2005.

[37] S. V. Gnedenkov and S. I. Sinebryukhov, "Electrochemical Impedance Spectroscopy of Oxide Layers on the Titanium Surface," *Russian Journal of Electrochemistry*, Volume 41, Number 8, 2005, Pages 858-865.

[38] G. A. Ragoisha and A. S. Bondarenko, " Potentiodynamic Electrochemical Impedance Spectroscopy for Solid State Chemistry." *Solid State Phenomena*, Volume 90-91.

[39] J. R. MacDonald, *Impedance Spectroscopy*, John Wiley & Sons, New York, 1987.

[40] R. Cottis and S. Turgoose, "Electrochemical Impedance and Noise," NACE International, Pages 1-111.

[41] Princeton Applied Research Application Notes AC-3, "Electrochemical Impedance Measurements: Instrumentation ad Techniques." http://www.princetonappliedresearch.com/

[42] Princeton Applied Research Application Notes AC-1, "Basics of Electrochemical Impedance Spectroscopy." http://www.princetonappliedresearch.com/

[43] Gamry Corrosion System Application Notes, "Basics of Electrochemical Corrosion Measurements." http://www.gamry.com/App_Notes/DC_Corrosion/